

Article

Optimization of Ultrasound-Assisted Cellulase Extraction from *Nymphaea hybrid* Flower and Biological Activities: Antioxidant Activity, Protective Effect against ROS Oxidative Damage in HaCaT Cells and Inhibition of Melanin Production in B16 Cells

Hui-Min Liu ^{1,2}, Sheng-Nan Lei ¹ , Wei Tang ¹, Meng-Han Xun ¹, Zhi-Wei Zhao ¹, Ming-Yan Cheng ¹, Xiao-Dan Zhang ³ and Wei Wang ^{1,2,*}

¹ School of Perfume & Aroma and Cosmetics, Shanghai Institute of Technology, Shanghai 201418, China; szliuhm@sit.edu.cn (H.-M.L.); 196071222@mail.sit.edu.cn (S.-N.L.); 216071129@mail.sit.edu.cn (W.T.); 206072134@mail.sit.edu.cn (M.-H.X.); 206071246@mail.sit.edu.cn (Z.-W.Z.); 206071241@mail.sit.edu.cn (M.-Y.C.)

² Engineering Research Center of Perfume & Aroma and Cosmetics, Ministry of Education, Shanghai 201418, China

³ Shanghai Shandai Biotechnology Co., Ltd., Qingpu District, Shanghai 201706, China; cncjay@126.com

* Correspondence: wangweittg@sit.edu.cn; Tel.: +86-189-1883-0550



Citation: Liu, H.-M.; Lei, S.-N.; Tang, W.; Xun, M.-H.; Zhao, Z.-W.; Cheng, M.-Y.; Zhang, X.-D.; Wang, W.

Optimization of Ultrasound-Assisted Cellulase Extraction from *Nymphaea hybrid* Flower and Biological Activities: Antioxidant Activity, Protective Effect against ROS Oxidative Damage in HaCaT Cells and Inhibition of Melanin Production in B16 Cells. *Molecules* **2022**, *27*, 1914. <https://doi.org/10.3390/molecules27061914>

Academic Editors: Andrei Mocan and Simone Carradori

Received: 3 March 2022

Accepted: 14 March 2022

Published: 16 March 2022

Publisher's Note: MDPI stays neutral with regard to jurisdictional claims in published maps and institutional affiliations.



Copyright: © 2022 by the authors. Licensee MDPI, Basel, Switzerland. This article is an open access article distributed under the terms and conditions of the Creative Commons Attribution (CC BY) license (<https://creativecommons.org/licenses/by/4.0/>).

Abstract: In this study, ultrasonic-assisted cellulase extraction (UCE) was applied to extract flavonoids and polyphenols from the *Nymphaea hybrid* flower. The extraction conditions were optimized using the response surface method (RSM) coupled with a Box-Behnken design. The crude extract of *Nymphaea hybrid* (NHE) was further purified using AB-8 macroporous resins, and the purified extract (NHEP) was characterized by FTIR and HPLC. In vitro activity determination by chemical method showed that NHEP displayed strong free radical scavenging abilities against the DPPH and ABTS radicals, good reduction power, and hyaluronidase inhibition. The cell viability by CCK-8 assays showed that NHEP had no significant cytotoxicity for B16 and HaCaT cells when the concentration was below 100 µg/mL and 120 µg/mL, respectively. NHEP with a concentration of 20–160 µg/mL can more effectively reduce the ROS level in H₂O₂ damaged HaCaT cells compared with 10 µg/mL of VC. The 40 µg/mL of NHEP had similar activity against intracellular melanin production in the B16 melanoma cells compared with 20 µg/mL Kojic acid. Good activities of antioxidation, whitening and protective effect against H₂O₂-induced oxidative damage promote the potential for NHEP as a functional raw material in the field of cosmetics and medicine.

Keywords: *Nymphaea hybrid*; ultrasound-assisted; cellulase; macroporous resins; antioxidant; ROS; melanin

1. Introduction

Nymphaea hybrid is a perennial aquatic herb of *Nymphaea* in *Nymphaeaceae* [1]. It is fragrant, colorful and indispensable as the main plant in features of water purification [2,3]. In the last few decades, scientists have paid more and more attention to *Nymphaea* and found that the extracts of some *Nymphaea* plants displayed good effects of antioxidation [4], whitening [5], antibiosis [6], anti-inflammation [7], liver protection [8], prevention of diabetes and dementia [9,10]. Flavonoids and polyphenols are mainly active substances of *Nymphaea*, which are impressive for the activities of good antioxidation and cell protection [4,11]. Therefore, in-depth study of flavonoids and polyphenols of *Nymphaea* has widespread application prospects in functional food, medicine and cosmetics industries. However, the studies about *Nymphaea hybrid* have been focused on the aromatic components for fragrance application, while there are only a few studies about flavonoids and polyphenols and other active ingredients.

A suitable extraction method is very important for preparing the natural plant active extracts. In recent years, experts have explored new methods of extraction that have a better extraction efficiency, enhanced greenness and shorter extraction time, such as microwave [12], ultrasonic [13], supercritical extraction [14] and enzymatic hydrolysis [15]. Ultrasound-assisted cellulase extraction (UCE) is one of the new methods that has been developed for the extraction of active ingredients from natural plants [16]. The basic principle of enzymatic extraction is to destroy the cell structure using an enzyme as a catalyst under mild reaction conditions so that the active ingredients can be released more quickly [17]. Besides, it has been reported that the enzyme activity can be enhanced by ultrasonic treatment under optimized conditions utilizing its thermal effect, mechanical fluctuant effect and cavitary effect [16]. UCE can not only improve the extraction efficiency but also enhance the quantity of the extracts [18–28]. As we know, there are few studies about extracting flavonoids and polyphenols from the *Nymphaea hybrid*, especially few reports on how to extract flavonoids sufficiently. Hence, in this paper, UCE coupled with the response surface method (RSM) was selected to develop the flavonoids and polyphenols extraction process of *Nymphaea hybrid*.

Natural plant extracts are usually complicated mixtures consisting of a variety of active ingredients. Recent research has shown that flavonoids and polyphenols are the largest groups of secondary metabolites of the *Nymphaea* extracts and are playing an important role in bioactivities [29]. The macroporous resins method is usually used for the further enrichment of active components from the crude extracts [30]. It has the advantages of high adsorption efficiency, simple operation, low cost, reusable and simple equipment [31–35].

Oxidative stress is one of the main risk factors in aging and most age-related diseases. It causes ROS levels to exceed the antioxidant capacity of cells, resulting in oxidative damage [36]. There are a considerable number of chemical [37] and cellular [38] tests for the evaluation of in vitro antioxidant activities of active ingredients for screening natural plant extracts. The chemical tests are easy to operate and have a low cost, which is commonly used for antioxidant and anti-inflammatory assays, such as DPPH, ABTS and other free radical scavenging assays, reduction power and hyaluronidase inhibition assay [39]. The cellular method is more and more prevalent by simulating the environment of the human body for the evaluation of antioxidants. Commonly used cells include fibroblasts, Human keratinocytes, and B16 cells [40]. More and more studies have been carried out into how active substances reduce the UVA/UVB or H₂O₂-induced oxidative stress in human cells [41].

The focus of this paper aims to (1) develop and optimize the ultrasound-assisted cellulase extraction process of the flavonoids from *Nymphaea hybrid* flower by RSM coupled with Box–Behnken design; (2) characterize the purified extract (NHEP) by FTIR and HPLC; (3) evaluate in vitro the bioactivities of extract assays to provide theoretical support for the product development and application of *Nymphaea hybrid* extract.

2. Results and Discussion

2.1. Single-Factor Experiments

The ultrasonic-assisted cellulase method was used to prepare NHE. The process included enzymatical hydrolysis with cellulase followed by ultrasonic extraction of flavonoids and polyphenols. Single-factor experiments and RSM were applied to optimize the preparation process. To explore the influence of different conditions, we developed four factors and five levels of an experimental program in the single-factor experiments. The factors including cellulase amount liquid-to-solid ratio, enzymatic hydrolysis time and ethanol concentration were selected to determine the influence on the content of flavonoids. As shown in Figure 1a, the flavonoid content first increases with the liquid-to-solid ratio from 20:1 (mL/g) to 40:1 (mL/g), then falls in the range of 40:1 (mL/g) to 60:1 (mL/g). The condition for the flavonoid content of NHE reached the maximum with the liquid-to-solid ratio of 40:1 (mL/g). The increasing contact area of solvent and solid is conducive to the diffusion of active substances [27], so the flavonoids content increases with the in-

crease of liquid-to-solid ratio. When the solvent is excessive, the effective concentration of cellulase and substrate concentration non-target active substance dissolved increased to reduce cellulase and substrate reduces, resulting in the flavonoid content of NHE dropping down [22,42]. Figure 1b showed that the flavonoid content increases as the cellulase amount increases from 2% to 4%, but the flavonoid content begins to decline when the addition amount of cellulase is higher than 4%. Cellulase could break down the cell wall into smaller molecules, which is conducive to the release of active substances. Excess cellulase might make a viscous enzyme solution which is not conducive to destroying the cell well and the enzymatic reaction process [43]. As shown in Figure 1c, the flavonoid content reaches a maximum at 60 min of enzymatic hydrolysis time. However, the flavonoid content did not change after 60 min, probably due to the diffusion equilibrium of flavonoids. The concentration of ethanol has an impact on the extraction rate of active components. The concentration of ethanol has an impact on the extraction rate of active components according to the principle of similar miscibility [43]. As shown in Figure 1d, the flavonoid content reaches a maximum when the concentration of ethanol was 50%.

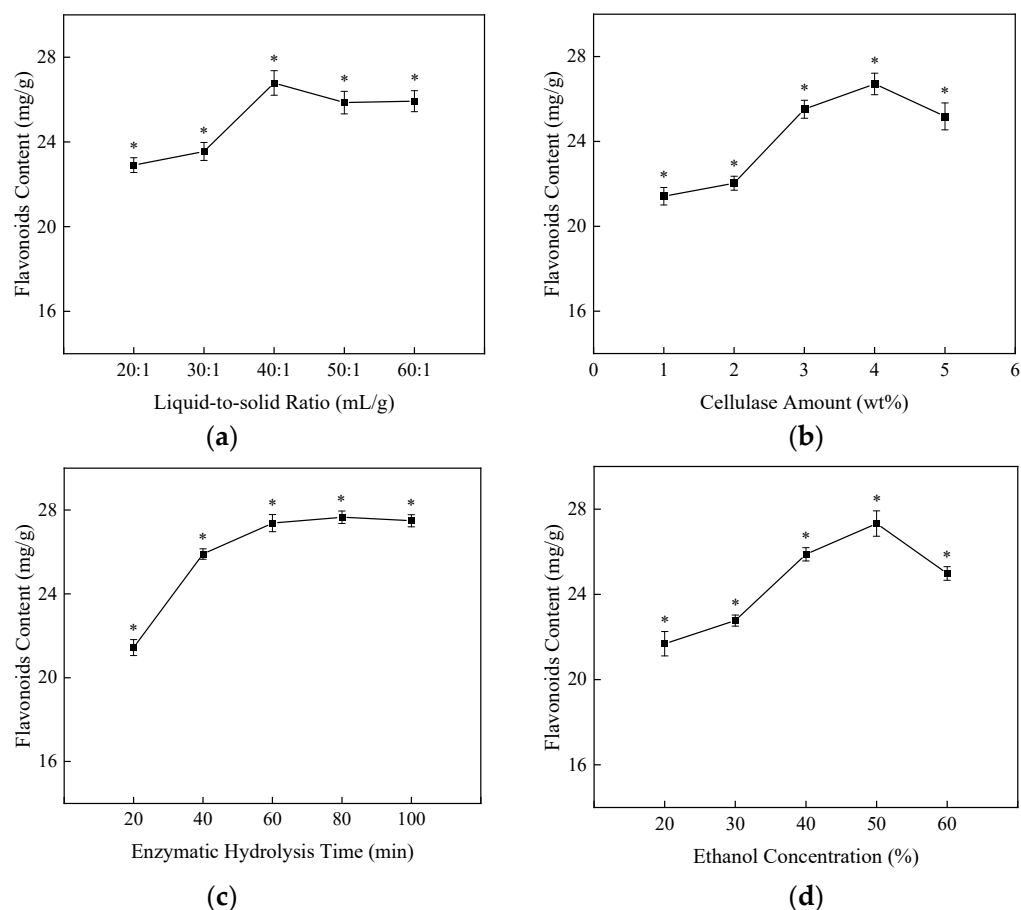


Figure 1. The influence of different factors on the content of flavonoids in NHE. (a) Liquid-to-solid ratio, (b) Cellulase amount (wt%), (c) Enzymatic hydrolysis time (min), (d) Ethanol concentration (%). The data shows as the mean \pm S.D. ($n = 3$). *: $p < 0.05$ compared between groups.

2.2. Response Surface Design

Based on the results of the single factor experiments, the liquid-to-solid ratio (A), cellulase amount (B) and ethanol concentration (C) were selected as the independent variables for optimizing the extraction process using the flavonoids content as an index. The results of the Box–Behnken experiment were shown in Table 1. According to different experiments, the flavonoids content of NHE was 20.67–27.06 mg/g. As in Table 2, multiple regression analysis was used to analyze the experimental data. Through the analysis

of the multivariate regression fitting, the relationship between the response variables (flavonoids content of NHE, Y) and the quadratic regression equation is shown in the formula as follows:

$$Y = 26.79 + 0.46A + 0.53B + 0.59C - 0.46AB - 0.39AC + 0.41BC - 3.03A^2 - 1.28B^2 - 1.67C^2 \quad (1)$$

Table 1. Scheme and experimental results of Box–Behnken.

NO.	A/(mL/g)	B/(%)	C/(%)	Flavonoids Content (mg/g)
1	40:1	4	50	26.62
2	40:1	5	60	25.66
3	30:1	3	50	21.30
4	40:1	5	40	23.34
5	40:1	3	40	22.83
6	50:1	4	60	22.73
7	40:1	4	50	26.40
8	40:1	4	50	27.06
9	30:1	4	60	22.30
10	50:1	4	40	22.65
11	30:1	4	40	20.67
12	40:1	4	50	26.92
13	30:1	5	50	23.02
14	50:1	3	50	22.85
15	40:1	4	50	26.95
16	50:1	5	50	22.72
17	40:1	3	60	23.52

Table 2. Variance analysis of Box–Behnken regression model results.

Source	Sum of Squares	df	Mean Squares	F-Value	p-Value
Model	71.7596	9	7.9733	67.6019	<0.0001 ***
A	1.6801	1	1.6801	14.2445	0.0069 **
B	2.2521	1	2.2521	19.0949	0.0033 **
C	2.7817	1	2.7817	23.5852	0.0018 **
AB	0.8540	1	0.8540	7.2411	0.0310 *
AC	0.5987	1	0.5987	5.0763	0.0589
BC	0.6680	1	0.6680	5.6636	0.0489 *
A ²	38.6989	1	38.6989	328.1105	<0.0001 ***
B ²	6.9468	1	6.9468	58.8986	0.0001 ***
C ²	11.7205	1	11.7205	99.3726	<0.0001 ***
Residual	0.8256	7	0.1179		
Lack of Fit	0.5251	3	0.1750	2.3293	0.2159
Pure Error	0.3006	4	0.0751		
Cor Total	72.5852	16			
R ²			0.9886		

R² = Coefficients of determination. Significance: * $p < 0.05$, ** $p < 0.01$ and *** $p < 0.001$.

The variance analysis of the Box–Behnken regression model results in Table 2 was obtained. The F-value of the equation model is 67.6, and the p -value is 0.0001 ($p < 0.001$), indicating that the model has an extremely significant statistical difference, and the model is meaningful. The high correlation coefficient value ($R^2 = 0.9886$) indicates that more than 98.86% of the response variability is explained by the model. The p -value of lack of fit is 0.2159, the F-value of lack of fit is 2.3293 and the three linear coefficients, three quadratic coefficients and two interaction terms are significant and interact. The results indicate that the quadratic regression model fitted well with the actual situation, and the model could be used to analyze the flavonoid content of NHE.

According to the result of regression analysis, the response surface 3D map and the contour plot maps were drawn in Figure 2. The 3D diagram can intuitively reflect the influence of the interaction of each factor on the response value, and through it, we can find the best parameters and the interactions among the parameters. According to the p -value, we can determine two interaction coefficients (AB, BC). Figure 2a shows the interaction between the liquid-to-solid ratio and the cellulase amount (AB) displayed significantly ($p < 0.05$). The flavonoid content increases with the increasing liquid-to-solid ratio and cellulase amount, while at a higher liquid-to-solid ratio (40:1–60:1 mL/g) and cellulase amount (4–6%), the interaction effect was not obvious. When the amount of cellulase reaches a certain point, the flavonoid content may decrease with the increase in cellulase amount and enlarge the liquid-to-solid ratio. The reason for this may be due to the appropriate cellulase amount and an enlargement of the liquid-to-solid ratio will improve the solubility and increase the mass transfer rate, but the excessive cellulase amount with too high a liquid-to-solid ratio will affect the reaction efficiency and mass transfer efficiency, resulting in a flavonoid content decrease with the liquid-to-solid ratio. A significant interaction effect ($p < 0.05$) between cellulase amount and ethanol concentration (BC) was also observed in Figure 2c.

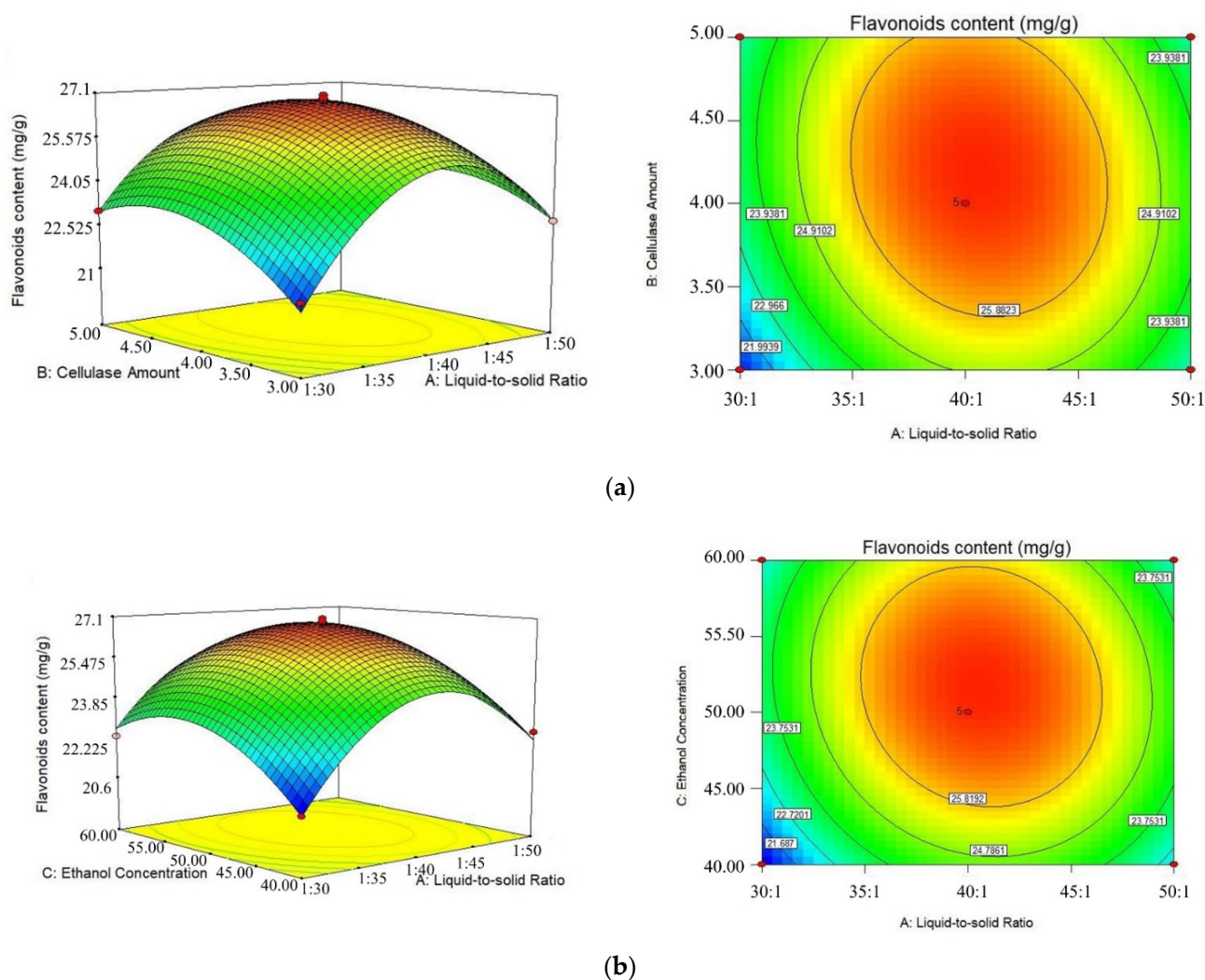


Figure 2. Cont.

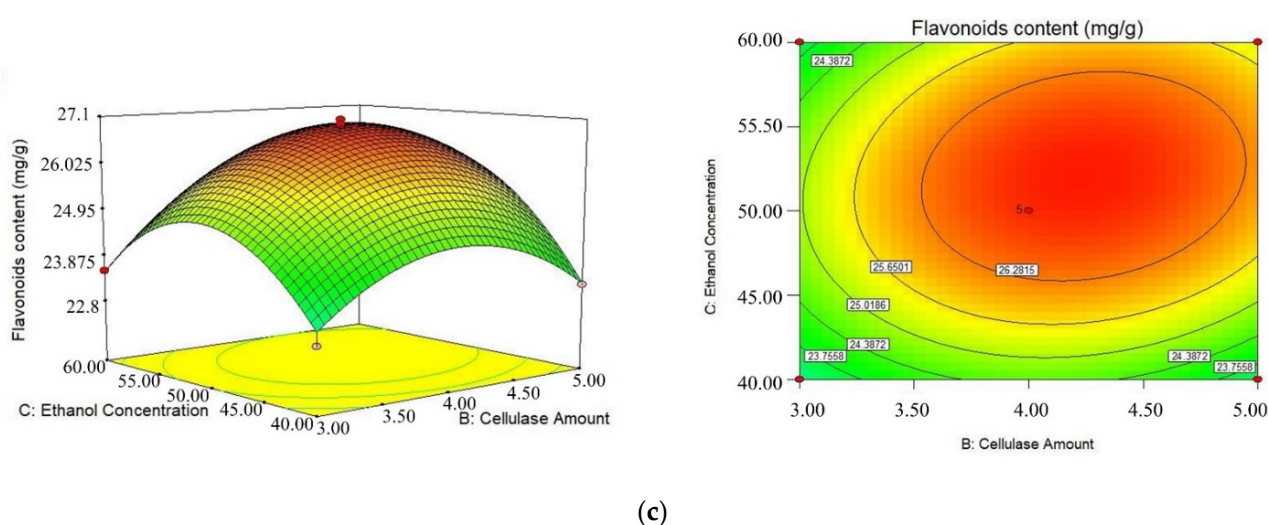


Figure 2. Response surface 3D and contour plots of different factors to effect the flavonoid content of NHE. (a) Liquid-to-solid ratio and cellulase amount; (b) Liquid-to-solid ratio and ethanol concentration; (c) Cellulase amount and ethanol concentration.

According to the response surface experiment, the optimal process conditions for extraction were as follows: the liquid-to-solid ratio was 40.45:1 (mL/g), cellulase amount was 5.23% (*w/w*), the ethanol concentration was 52% (*v/v*). Under such conditions, the predicted flavonoid content of NHE was 26.92 mg/g. To verify these optimal conditions, the experiment was repeated five times and the average actual flavonoid content of NHE was 27.26 ± 0.64 mg/g ($n = 5$), which was close to the predicted value and proved the validity of the models.

2.3. AB-8 Macroporous Resin

2.3.1. Static Adsorption and Desorption

The static adsorption and desorption curves of AB-8 macroporous resin for the flavonoid content of NHE were shown in Figure 3. As shown in Figure 3, the adsorption capacity of resin AB-8 is greater at 0–80 min; the adsorption capacity is slowly increasing at 80–240 min; and the adsorption capacity is not changed significantly after 240 min. This suggests that the adsorption equilibrium occurred and the adsorption capacity was 16.35 ± 0.25 mg/g ($n = 3$). The flavonoids into the resin AB-8 were desorbed, and the desorption ratio increased rapidly first and then slowed down within the first 240 min. After 240 min, the flavonoid content in the solution of desorption did not change significantly when the desorption capacity was 15.61 ± 0.25 mg/g ($n = 3$).

The effects were determined with pH (Figure 3b), sample concentration (Figure 3c), ethanol concentration (Figure 3d) on the static adsorption and desorption experiments. The solutions of NHE were adjusted to a different pH value (2.0, 3.0, 4.0, 5.0 and 6.0) by using 2.0 mol/L HCl and 2.0 mol/L NaOH solutions. Because flavonoids have a phenolic hydroxyl structure and are acidic, they can exist in a molecular state and can be absorbed into the resin by van der Waals force under the condition of the weak acid [44]. Therefore, the flavonoid content was highest at pH = 3. The solutions of NHE were diluted with distilled water to different concentrations (0.33, 0.49, 0.65, 0.82, 0.98 and 1.15 mg/mL). With the increase in concentration of the sample solution, the flavonoid adsorption capacity of resin AB-8 increased first and then remained stable. The high concentration of the sample solution blocked resin adsorption due to the interaction of the hydroxyl of flavonoids with water. The adsorption capacity of the high solution decreased due to the increase in impurities in the solution [33,45].

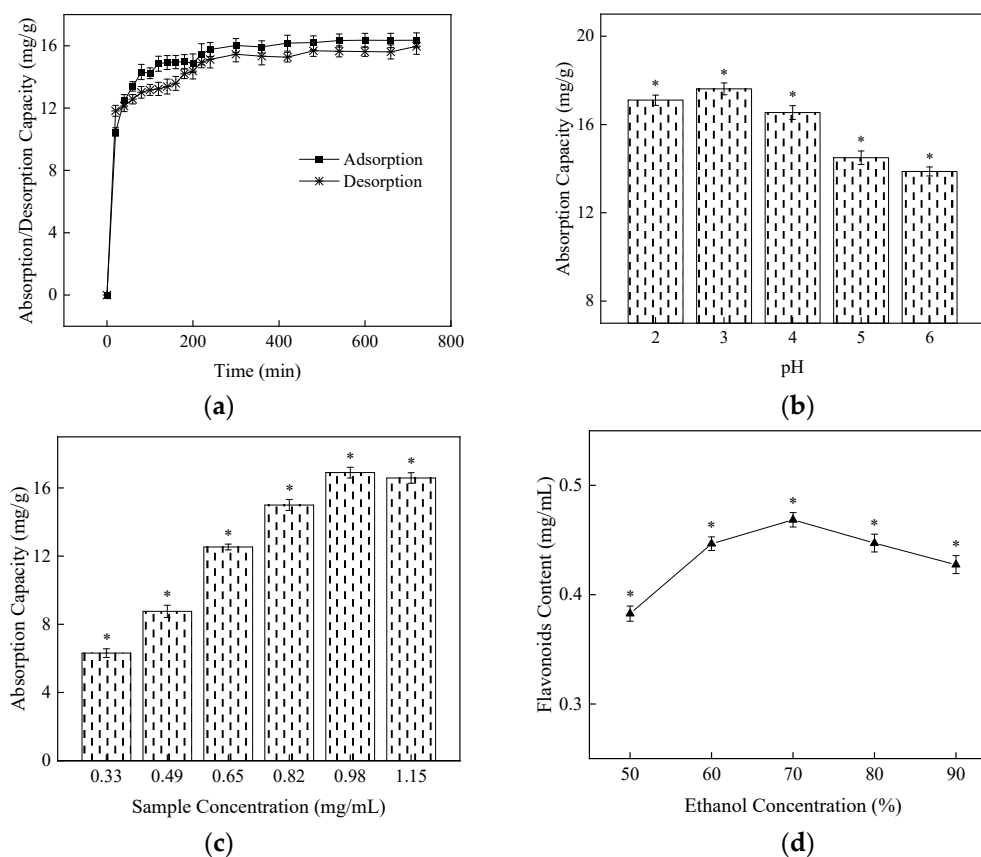


Figure 3. Effects of different factors on static adsorption and desorption of AB-8. (a) Adsorption and desorption curve; (b) Influence of pH on adsorption; (c) Influence of sample concentration on adsorption; (d) Influence of ethanol concentration on desorption. The data shows as the mean \pm S.D. ($n = 3$). *: $p < 0.05$ compared between groups.

Ethanol is commonly used as an eluent. It has a good solubility for flavonoids. A small amount of water solution can dissolve the part of water-soluble components and improve the desorption of flavonoids [33,46]. The adsorbed flavonoids into the resin AB-8 were desorbed with ethanol of different concentrations (50%, 60%, 70%, 80%, 90%). As shown in Figure 3d, with the increase of ethanol concentration, the flavonoid content of the solution was increased first and then decreased. The 70% (v/v) was the optimum ethanol concentration.

2.3.2. Dynamic Adsorption and Desorption

The influence of sample volume (a) and adsorption flow velocity (b) were determined on the dynamic adsorption capacity of flavonoids into the resin AB-8 in Figure 4. The abscissa was the sample volume, and the ordinate was the flavonoid concentration of the sample solution after adsorption. As shown in Figure 4a, with the increase of sample volume, the adsorption capacity of AB-8 decreased in the range of 0–70 mL and then did not significantly change in the range of 70–120 mL. The adsorption capacity of resin AB-8 was limited, while the appropriate adsorption volume can effectively improve [33]. Figure 4b shows that the samples were into the resin AB-8 with the flow rate of 1.2–7.2 BV/h, in which the adsorption capacity of AB-8 decreased on the NHE flavonoids. When the flow rate was too high, some active components were not adsorbed by the resin AB-8 and leaked out [47]. The changing trend of flavonoid concentration was similar in the effluent at 1.2 BV/h and 2.4 BV/h. Therefore, the flow rate of 2.4 BV/h was selected for adsorption with higher efficiency.

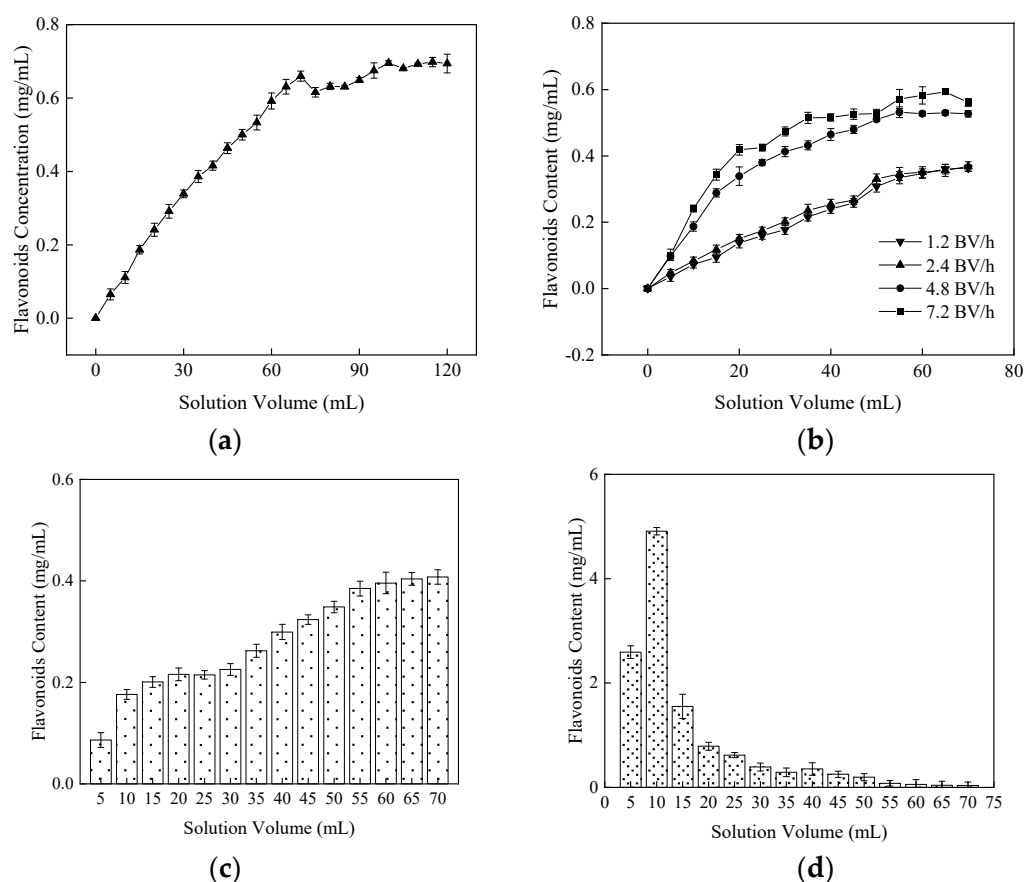


Figure 4. Effects of different factors on dynamic adsorption and desorption of AB-8. (a) Sample volume, (b) Adsorption flow velocity, (c) Adsorption and (d) Desorption curve. The data are shown as the mean \pm S.D. ($n = 3$). The volume of the resin bed (BV) is 25 mL.

The dynamic adsorption (c) and desorption (d) curves were drawn in Figure 4. The concentration of flavonoids of effluent was increased gradually at the flow rate of 2.4 BV/h. When the sample volume was 70 mL in Figure 4c, the flavonoid capacity in the effluent solution did not change significantly. As shown in Figure 4d, the flavonoids into the resin AB-8 were firstly increased and then decreased with the eluent of 70% ethanol. When the flavonoids concentration of eluent resolution approached zero, the adsorbed flavonoids of resin AB-8 were completely eluted.

NHEP was prepared by the purification of NHE with AB-8 macroporous resin. As shown in Table 3, the content of flavonoids and polyphenols in the NHEP sample was higher than in the NHE sample with the same dry weight. After purification, the contents of flavonoids and polyphenols in NHEP increased from 55.60 mg/g to 157.39 mg/g and from 414.97 mg/g to 888.63 mg/g, respectively. This result showed that it was efficient for the enrichment of flavonoids and polyphenols of NHE by AB-8 macroporous resin.

Table 3. The content of flavonoids and polyphenols in the NHE and NHEP with the same dry weight.

Sample	Compound	
	Flavonoids Content (mg/g)	Polyphenols Content (mg/g)
NHE	55.60 \pm 0.38	414.97 \pm 2.95
NHEP	157.39 \pm 1.18 *	888.63 \pm 4.41 *

The data shows as the mean \pm S.D. ($n = 3$). *: $p < 0.05$ compared to NHE.

2.4. Activity Determination by Chemical Method

To explore in vitro antioxidant activity of NHE and NHEP, the free radical scavenging abilities against ABTS, DPPH, and reduction power, were detected compared with VC. As shown in Figure 5, the IC_{50} values of the DPPH radical of NHE, NHEP and VC were $11.09 \pm 0.15 \mu\text{g/mL}$, $3.28 \pm 0.03 \mu\text{g/mL}$ and $5.18 \pm 0.06 \mu\text{g/mL}$, respectively. The IC_{50} values of the ABTS radical of NHE, NHEP and VC were $18.21 \pm 0.05 \mu\text{g/mL}$, $10.50 \pm 0.10 \mu\text{g/mL}$ and $7.77 \pm 0.04 \mu\text{g/mL}$, respectively. The reduction power of NHE, NHEP, VC for Fe^{3+} were strong with high absorbances [48]. The absorbances were 2.20 ± 0.04 , 2.36 ± 0.04 and 2.60 ± 0.07 in the 1 mg/mL concentration, respectively. This result indicated that the scavenging free radical abilities and reduction power of NHEP were similar to VC and stronger than that of NHE. NHE and NHEP were also evaluated for the anti-inflammatory activity by using hyaluronidase inhibition assays. The IC_{50} value of NHE and NHEP in hyaluronidase inhibition assay was $0.55 \pm 0.01 \text{ mg/mL}$ and $0.32 \pm 0.01 \text{ mg/mL}$. The inhibition rate of $10 \mu\text{g/mL}$ dipotassium glycyrrhizinate (Dg) was $94.23 \pm 1.72\%$. This result showed that both NHE and NHEP display an anti-inflammatory effect, and NHEP has a stronger anti-inflammatory effect than NHE. Hence, in vitro bioactivity evaluation by chemical assays showed that both NHE and NHEP displayed strong free radical scavenging abilities against the DPPH and ABTS radicals, good reduction power, and anti-inflammatory effect.

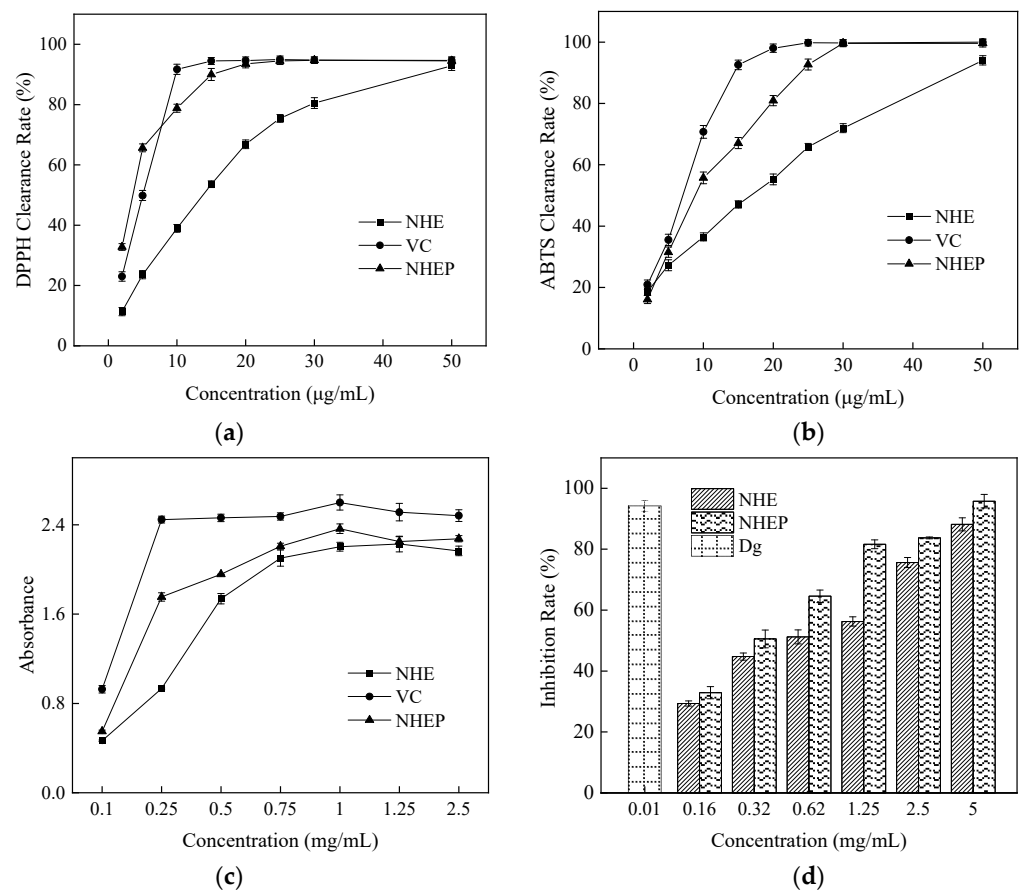


Figure 5. Activities of the NHE, NHEP and positive control by chemical method. (a) DPPH, (b) ABTS, (c) Reduction power, (d) Hyaluronidase inhibition assay. Dg stands for Dipotassium glycyrrhizinate, and the concentration is $10 \mu\text{g/mL}$. The data is shown as the mean \pm S.D. ($n = 3$).

2.5. Characterization of FTIR and HPLC

Infrared spectroscopy analysis can be used as a powerful tool to characterize and identify functional groups present in the compounds. As shown in Figure 6, the absorption peak at the vicinity of 3424 cm^{-1} is relatively wide and strong, which is attributed to the stretching vibration of O–H. The signal in wavelength of 2930 cm^{-1} is assigned to the absorption peak of stretching vibration of the C–H bond of aliphatic hydrocarbon [49]. The band at $3000\text{--}3100\text{ cm}^{-1}$ is due to the stretching vibration of C–H of the aromatic ring. The aromatic C–H bond was out-of-plane bending vibration, resulting in absorption peaks at 834 and 760 cm^{-1} wavelengths [50]. A characteristic absorption peak at 1718 cm^{-1} may be assigned to the carboxylic acid of a sharp stretching band of the C=O. The peaks at 1613 and 1449 cm^{-1} wavelength belong to the C=C bond of the aromatic ring vibrates [51]. The absorption peaks at 1512 cm^{-1} may be assigned to the aromatic skeletal vibrations, ring breathing with C–O stretching vibration [50]. The adsorption peaks at 1449 and 1349 cm^{-1} are assigned to the bending vibrations of $-\text{CH}_3$ and $-\text{CH}_2$. The peaks at 1210 and 1038 cm^{-1} wavelength belong to the stretching vibration of C–H and C–O bonds [52]. The characteristic peaks of the benzene ring, C–O stretching vibration and stretching vibration of O–H, indicate the presence of phenolic hydroxy groups [53].

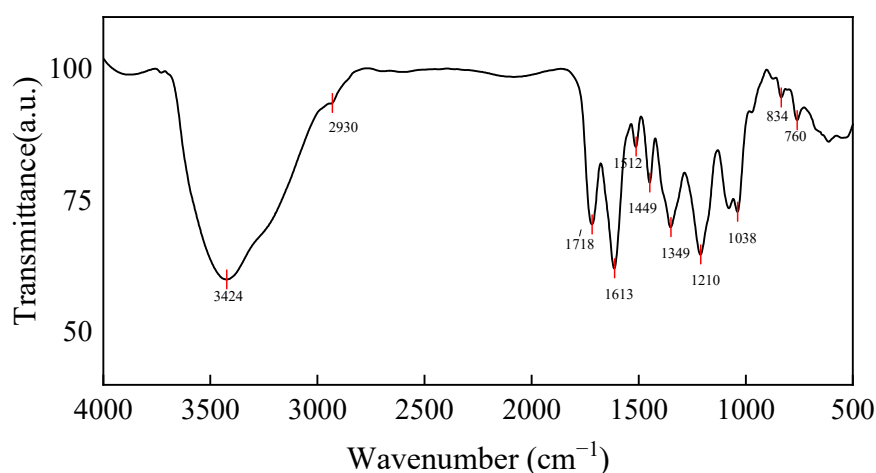


Figure 6. FTIR-NHEP illustrating structural features.

The total polyphenol and flavonoid compositions of NHEP were identified by the characterization of HPLC in Figure 7 and Table 4. This result showed some of the main NHEP bioactive phytochemicals, including gallic acid ($1.60 \pm 0.36\text{ mg/g}$), corilagin ($65.60 \pm 3.36\text{ mg/g}$), ellagic acid ($97.72 \pm 0.92\text{ mg/g}$), rutin ($34.41 \pm 4.24\text{ mg/g}$), myricetin ($3.13 \pm 0.87\text{ mg/g}$), quercetin ($4.64 \pm 0.15\text{ mg/g}$), naringin ($4.03 \pm 0.24\text{ mg/g}$) etc. The contents of corilagin, ellagic acid and rutin in NHEP were higher among these components. These standard substances have been reported to have excellent antioxidant activity, which further indicated that NHEP has great potential as a natural antioxidant. Uddin et al. identified 9 bioactive phytochemicals from methanolic extract of *Nymphaea nouchali* using an HPLC system [54]. Among these compounds, rutin (39.44 mg/g), myricetin (30.77 mg/g), ellagic acid (11.05 mg/g), gallic acid (5.33 mg/g) and quercetin (0.90 mg/g) were polyphenols or flavonoids, which were also identified as bioactive ingredients of NHEP in this work. We found the ellagic acid content ($97.72 \pm 0.92\text{ mg/g}$) of NHEP was much greater than that (11.05 mg/g) of *Nymphaea nouchali* and that ($6.16 \pm 0.019\text{ mg/g}$) of ethanolic extract of Water Lily (*Nymphaea Tetragona Georgi*) [55].

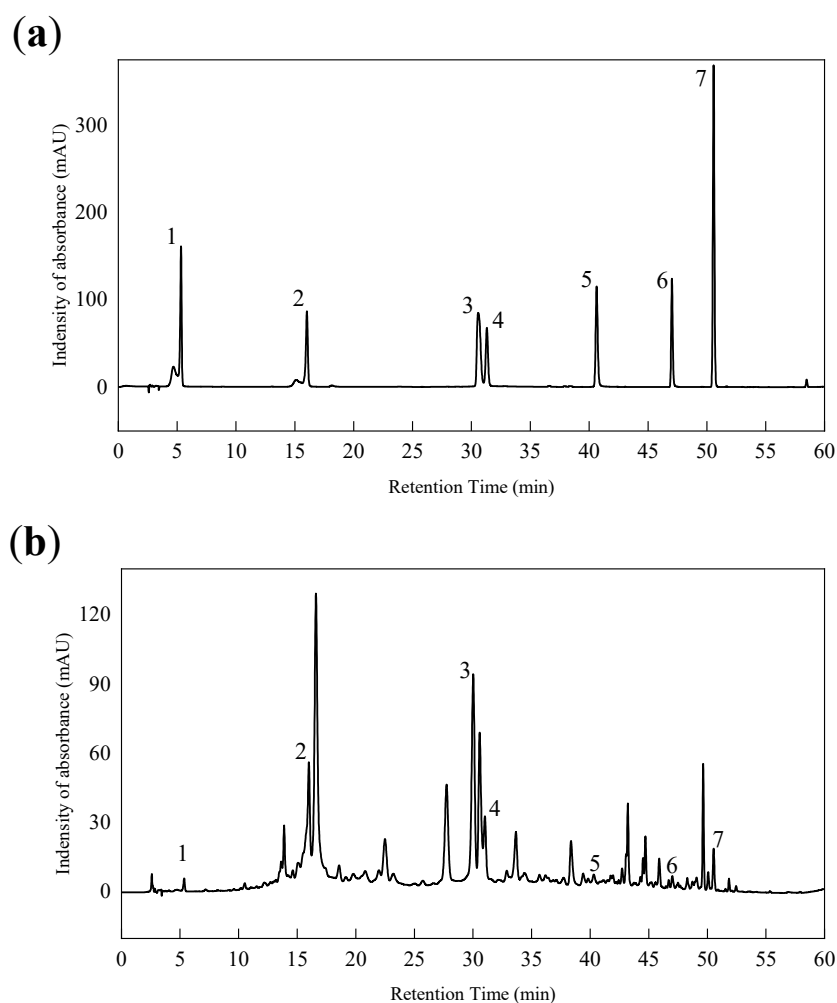


Figure 7. HPLC of mixed standards (a) and NHEP (b). 1-gallic acid, 2-corilagin, 3-ellagic acid, 4-rutin, 5-myricetin, 6-quercetin, 7-naringin.

Table 4. Polyphenols and flavonoids compositions of NHEP by the characterization of HPLC.

Standard	Retention Time (min)	Regression Equation	R ²	NHEP Compound (mg/g)
Gallic acid	5.33	$y = 28.696x - 6.5794$	0.9997	1.60 ± 0.36
Corilagin	16.21	$y = 14.902x - 40.435$	0.9992	65.60 ± 3.36
Ellagic acid	30.58	$y = 10.3x - 11.978$	0.9999	97.72 ± 0.92
Rutin	31.32	$y = 10.71x - 9.2865$	0.9999	34.41 ± 4.24
Myricetin	40.86	$y = 12.76x + 4.3092$	0.9996	3.13 ± 0.87
Quercetin	47.15	$y = 11.001x + 2.6758$	0.9999	4.64 ± 0.15
Naringin	50.69	$y = 34.715x + 24.424$	0.9999	4.03 ± 0.24

Y = The peak area (mAU*s); X = The concentration of standards ($\mu\text{g}/\text{mL}$); R² = Coefficients of determination. The data shows as the mean \pm S.D. ($n = 3$).

2.6. HaCaT Cells Experiments

2.6.1. Effects of NHEP and H₂O₂ on Cell Viability of HaCaT Cells

CCK-8 kit assay was used to determine the cytotoxicity of NHEP and H₂O₂ on HaCaT cells. As shown in Figure 8a, HaCaT cells were cultured with NHEP in the concentration range of 10–120 $\mu\text{g}/\text{mL}$ for 24 h, and the cell viability was higher than 90% of the control group, indicating that there was no cytotoxicity. The higher the dose of NHEP, the lower the cell viability observed. When the concentration of NHEP rose to 160 $\mu\text{g}/\text{mL}$ and 200 $\mu\text{g}/\text{mL}$, the cell viability decreased to $88.79\% \pm 2.64\%$ ($p < 0.001$) and $81.14\% \pm 3.66\%$ ($p < 0.001$). As shown in Figure 8b, the culture time of the cells treated with NHEP in the

same concentration range was extended from 24 h to 48 h. The cell viability was higher than 90% of the control group in the NHEP concentration range of 10–80 $\mu\text{g}/\text{mL}$. The cell viability decreased gradually when the concentration of NHEP increased to 120 $\mu\text{g}/\text{mL}$ ($88.17\% \pm 5.16\%$, $p < 0.001$), 160 $\mu\text{g}/\text{mL}$ ($80.75\% \pm 4.87\%$, $p < 0.001$) and 200 $\mu\text{g}/\text{mL}$ ($72.85\% \pm 3.58\%$, $p < 0.001$). We can obviously find that while the culture time of the cells extended, the cytotoxicity significantly increased as the cell viability decreased by 10.81%, 8.04%, 8.29%, respectively when the cells were treated with a higher concentration of NHEP (120–200 $\mu\text{g}/\text{mL}$). The CCK-8 assay results were consistent with cell growth density and cellular morphology, as shown in Figure 8c. Therefore, with the concentration of NHEP being higher and the incubation time of HaCaT being longer, the cytotoxicity of cells was stronger, affecting cell growth activity and resulting in cell shedding and death [56].

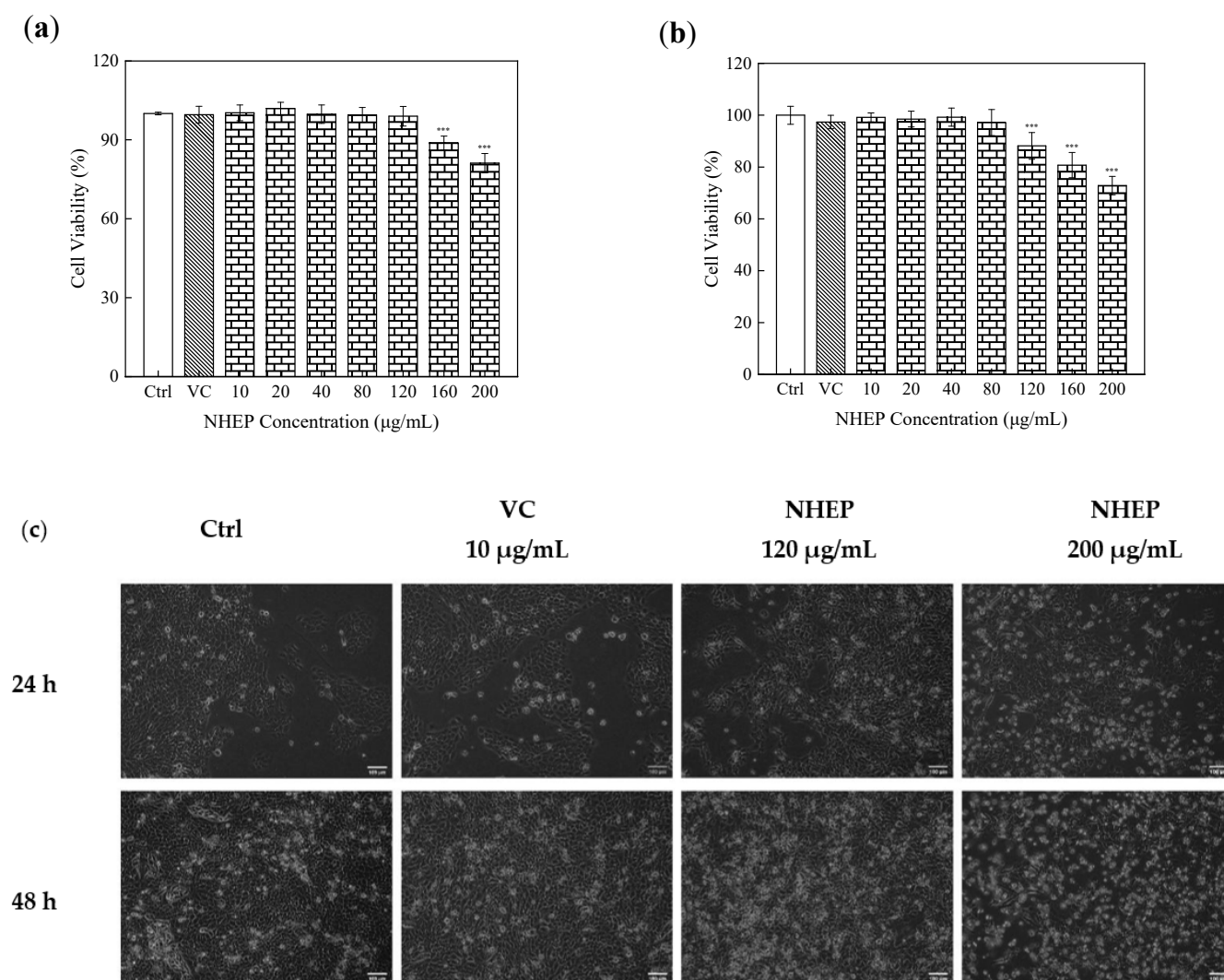


Figure 8. Cytotoxicity of NHEP on HaCaT cells. (a) cell viability of the HaCaT cells cultured with the NHEP for 24 h, (b) cell viability of the HaCaT cells cultured with the NHEP for 48 h, (c) cellular morphology of the HaCaT cells cultured with the NHEP for 24 h and 48 h (scale bar is 100 μm). VC stands for Vitamin C, and the concentration is 10 $\mu\text{g}/\text{mL}$. Significance: compared with the control group, *** $p < 0.001$. The data shows as the mean \pm S.D. ($n = 5$).

H_2O_2 can be used as an inducer to promote intracellular ROS production in certain concentrations [57]. In order to confirm an appropriate concentration for the H_2O_2 -induced injury model in vitro, the nominal concentration of H_2O_2 (25–300 μM) exposed to HaCaT cells was assessed by the CCK-8 kit. As shown in Figure 9a, the cell viability of HaCaT

cells decreased gradually to 50% ($p < 0.001$) with a concentration of H_2O_2 increased to 100 μM . Therefore, 100 μM of H_2O_2 was selected to induce cellular ROS oxidation damage on HaCaT cells in the subsequent experiments.

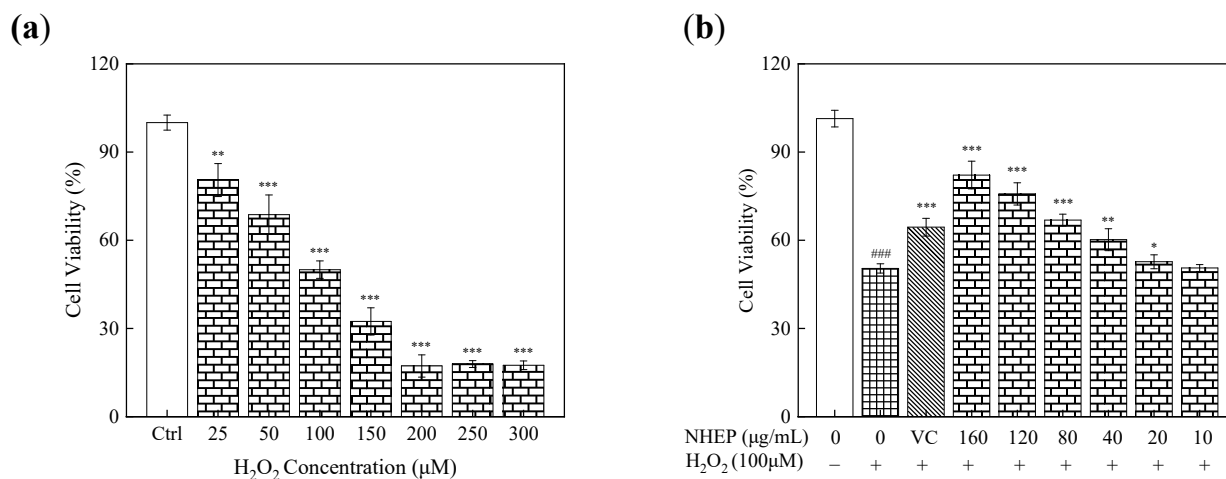


Figure 9. Cytotoxicity of H_2O_2 and NHEP on HaCaT cells. (a) viability of the HaCaT cells cultured with the H_2O_2 , (b) viability of the HaCaT cells cultured with H_2O_2 and NHEP. VC stands for Vitamin C, and the concentration is 10 $\mu g/mL$. Significance: ### $p < 0.001$ compared with the control group. * $p < 0.05$, ** $p < 0.01$, *** $p < 0.001$ compared with the H_2O_2 stimulation group. The data shows as the mean \pm S.D. ($n = 5$).

As shown in Figure 9b, HaCaT cells were cultured first with 10–200 $\mu g/mL$ NHEP and then treated with 100 μM H_2O_2 for 2 h. Compared with the control group treated only with H_2O_2 , HaCaT cells had higher cell viability when pretreated with NHEP in the range of 20–160 $\mu g/mL$. The higher concentration of NHEP, the higher the HaCaT cell viability. The cell viabilities of HaCaT cells cultured with 20, 40, 80, 120, 160 $\mu g/mL$ NHEP were 52.66% \pm 2.36% ($p < 0.05$), 60.19% \pm 3.71% ($p < 0.01$), 66.85% \pm 2.00% ($p < 0.001$), 75.77% \pm 3.79% ($p < 0.001$) and 82.17% \pm 4.70% ($p < 0.001$), respectively. Although 160 $\mu g/mL$ NHEP had a low cytotoxicity compared with HaCaT cells, it displayed a better inhibition against the stimulation of H_2O_2 . The cell viabilities of 80–160 $\mu g/mL$ NHEP pretreatment groups were higher than that of the 10 $\mu g/mL$ VC pretreatment group (64.44% \pm 3.00%, $p < 0.001$). It was reported that polyphenols and flavonoids can effectively inhibit the generation of intracellular ROS and protect cells against oxidative damage [41]. In this case, the content of polyphenols and flavonoids increased with the increase of NHEP concentration. The polyphenols and flavonoids of NHEP may positively contribute to the protection of HaCaT cells against oxidative damage induced by H_2O_2 .

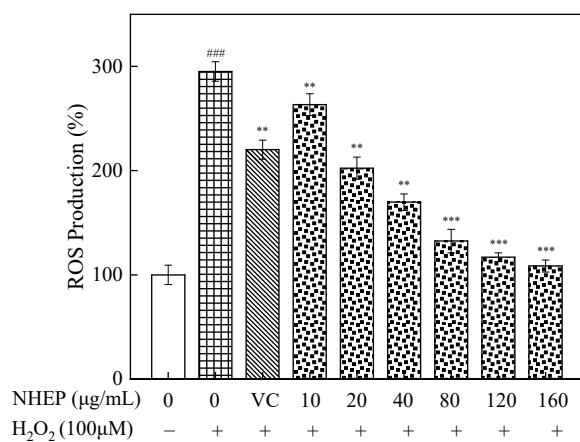
2.6.2. Effects of NHEP on the ROS Level of HaCaT Cells with Stimulation of H_2O_2

Excessive ROS may destroy the structural integrity of the cell and eventually lead to oxidative damage of organisms [57]. H_2O_2 is a precursor of many radicals and can increase the intracellular ROS levels by crossing the cell membrane [58,59]. In this study, the HaCaT cells were first induced to produce ROS with 100 μM H_2O_2 and then treated with NHEP of different concentrations.

The effect of intracellular ROS level in the HaCaT cells was detected by a fluorescent probe DCFH-DA. The percentage of ROS proportion was taken in the control group as the index. As shown in Figure 10, the ROS levels and fluorescent intensity in HaCaT cells significantly increased after the stimulation of H_2O_2 . The ROS levels of the stimulated injury group were 295.17% \pm 9.29% ($p < 0.001$), which is significantly higher than that of the control group and NHEP post-treatment groups. With the increasing concentration of NHEP, the ROS levels reduced gradually, indicating that NHEP in the concentration range of 10–160 $\mu g/mL$ can efficiently inhibit the ROS production in HaCaT cells stimulated by

H₂O₂. The ROS levels of 20–160 µg/mL NHEP groups were lower than that of the VC group (220.17% ± 9.12%, $p < 0.01$), and displayed weaker fluorescence intensity. The ROS production of 20–160 µg/mL NHEP were 202.35% ± 10.65% ($p < 0.01$), 169.74% ± 7.88% ($p < 0.01$), 132.43% ± 11.25% ($p < 0.001$), 116.87% ± 4.22% ($p < 0.001$) and 108.52% ± 5.75% ($p < 0.001$), respectively. In conclusion, NHEP has a better protection ability antioxidative damage. NHEP can effectively reduce the ROS levels in HaCaT cells induced by H₂O₂ so that NHEP has good cell protection against oxidative damage in the range of 20–120 µg/mL.

(a)



(b)

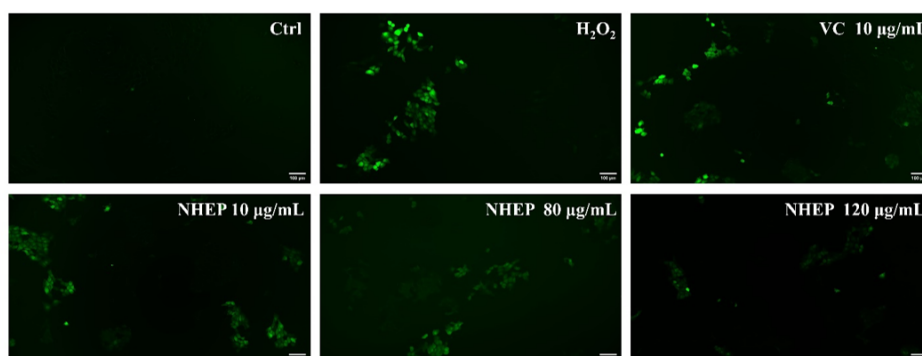


Figure 10. Effects of NHEP on the ROS level of HaCaT cells with stimulation of H₂O₂: (a) ROS production, (b) fluorescence intensity by detected the DCFH-DA. VC stands for Vitamin C, and the concentration is 10 µg/mL (scale bar is 100 µm). Significance: ### $p < 0.001$ compared with the control group. ** $p < 0.01$, *** $p < 0.001$ compared with the H₂O₂ stimulation group. The data are shown as the mean ± S.D. ($n = 5$).

2.7. B16 Cell Experiments

2.7.1. Activity of B16 Cells

The cytotoxicity of 10–140 µg/mL NHEP on B16 cells was determined by the CCK-8 kits. As shown in Figure 11a, B16 cells were cultured with 10–140 µg/mL NHEP for 24 h. The result showed that it was no significant cytotoxicity with the cell higher than 90% in the NHEP concentration range of 10–120 µg/mL. The cell viability decreased to 84.66% ± 3.45% ($p < 0.001$) when the NHEP concentration was 140 µg/mL. As shown in Figure 11b, B16 cells were cultured with 10–140 µg/mL NHEP for 48 h, and results showed that it was not significant with the cell viability higher than 90% in the NHEP concentration range of 10–100 µg/mL. The cell viabilities of 100, 120 and 140 µg/mL decreased to 89.07% ± 3.17% ($p < 0.001$), 72.98% ± 2.96% ($p < 0.001$) and 63.54% ± 3.73% ($p < 0.001$), respectively. Comparing the results of different culture times, we can obviously find that

the culture time of the cells extended the cytotoxicity increased significantly with cell viability decreased by 10.79%, 18.26% and 21.11%, respectively, when the cells were treated with a higher concentration of NHEP (100–140 $\mu\text{g}/\text{mL}$). It was reported that flavonoids and polyphenols would affect anti-tumor cell proliferation and apoptosis [60,61]. In conclusion, with the increase in concentration and incubation time, the cytotoxicity of B16 cells was significantly enhanced. As shown in Figure 11c, the cell growth density decreased at high concentrations. The results were consistent with the data reported by Teng et al. that a high concentration of *Nymphaea* extract may induce apoptosis of B16 cells [62,63].

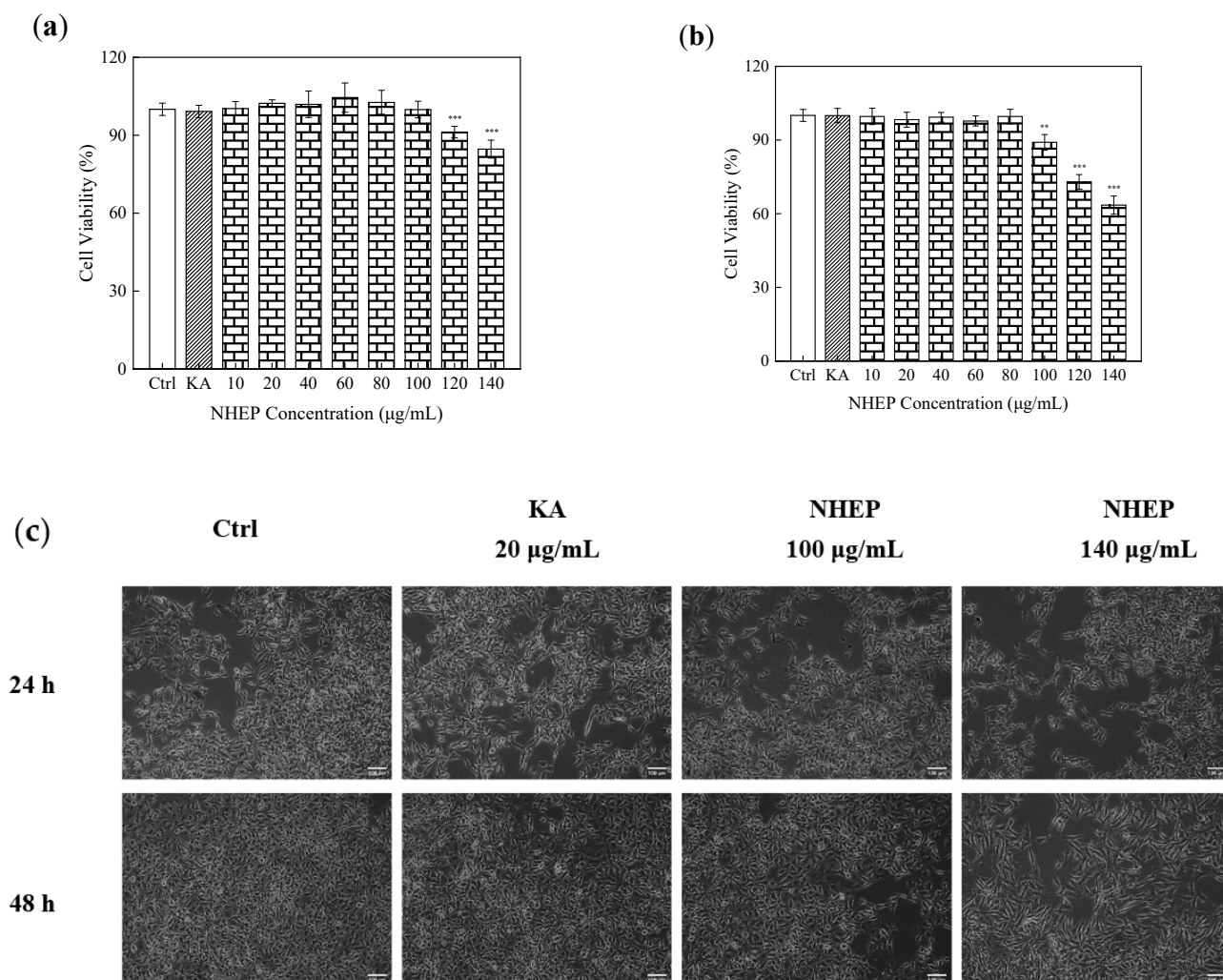


Figure 11. Cytotoxicity of NHEP on B16 cells: (a) viability of the B16 cells cultured with the NHEP for 24 h, (b) viability of the B16 cells cultured with the NHEP for 48 h, (c) cellular morphology of the B16 cells cultured with the NHEP for 24 h and 48 h (scale bar is 100 μm). Significance: compared with the control group, ** $p < 0.01$, *** $p < 0.0001$. The data shows as the mean \pm S.D. ($n = 5$). KA stands for Kojic acid, and the concentration is 20 $\mu\text{g}/\text{mL}$.

2.7.2. Effects of NHEP on B16 Melanin Production

As shown in Figure 12, 10–140 $\mu\text{g}/\text{mL}$ NHEP effectively inhibited the melanin production on B16 cells, and the higher concentration of NHEP and the stronger the inhibition ability. This result indicated that NHEP has a better effect on whitening by inhibiting melanin production. When B16 cells were cultured with NHEP in the range of 10–80 $\mu\text{g}/\text{mL}$ for 24 h or 48 h and no significant cytotoxicity. The melanin content of B16 cells was $67.35\% \pm 2.36\%$ ($p < 0.001$) when treated with 40 $\mu\text{g}/\text{mL}$ NHEP. A similar melanin content of B16 cells ($68.57\% \pm 4.47\%$, $p < 0.001$) was produced in contrast with the positive con-

trol group (20 $\mu\text{g}/\text{mL}$ KA). When the NHEP concentration increased to 100–140 $\mu\text{g}/\text{mL}$, the melanin content obviously decreased to $42.65\% \pm 2.34\%$ ($p < 0.001$), $36.53\% \pm 1.81\%$ ($p < 0.001$) and $24.69\% \pm 5.18\%$ ($p < 0.001$), respectively. This may be due to the fact that NHEP can induce apoptosis of B16 cells or inhibit tyrosinase activity [62,63].

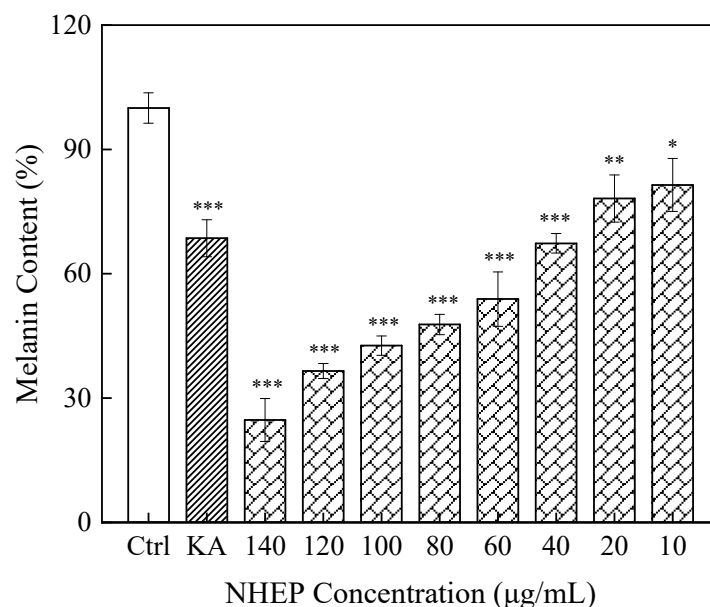


Figure 12. Effects of the NHEP on B16 cells melanin production. Significance: compared with the control group, * $p < 0.05$, ** $p < 0.01$, *** $p < 0.001$. The data shows as the mean \pm S.D. ($n = 5$). KA stands for Kojic acid, and the concentration is 20 $\mu\text{g}/\text{mL}$.

3. Materials and Methods

3.1. Materials

Nymphaea hybrid flowers were purchased from the Liandao Agricultural Development Co., Ltd. (Shanghai, China). *Nymphaea hybrid* flowers were rinsed with distilled water and frozen. Then, the frozen *Nymphaea hybrid* flowers were placed into a vacuum freeze-dryer (TF-FD-1, Tuoyuan Co., Ltd., Shanghai, China) for freeze-drying to a constant weight. Then *Nymphaea hybrid* flowers were crushed into a fine powder (50 mesh) by a shredder and stored in air-sealed bags at a low temperature ($-20\text{ }^{\circ}\text{C}$) for use. The AB-8 macroporous resins were purchased from the San Xing Resin Co., Ltd. (Anhui, Bengbu, China).

3.2. Chemical Reagents

Ultrapure water, anhydrous ethanol, Folin-phenol, AlCl_3 , Na_2CO_3 , HCl, NaOH, CaCl_2 , NaH_2PO_4 , Na_2HPO_4 , KBr, acetic acid, sodium acetate, acetylacetone, 4-Dimethylaminobenzaldehyde, DPPH, ABTS, Dipotassium glycyrrhizinate, cellulase, potassium persulfate, hyaluronidase (Sigma, H3506, Shanghai, China), sodium hyaluronate (Sigma, H5388, Shanghai, China), DMEM, CCK-8 assay, PBS, pancreatin, reactive oxygen species assay kit, H_2O_2 , methanol, formic acid, acetonitrile and other chemicals, rutin standard, gallic acid standard, ellagic acid standard, corilagin standard, myricetin standard, quercetin standard, naringin standard, all reagents is analytical grade. All reagents, solvents and standards were purchased from MACKLIN (Shanghai, China). HaCaT cells and B16 mouse melanoma cells were purchased from the Shanghai Cell Bank of the Chinese Academic of Sciences.

3.3. Preparation of NHE

NHE was prepared by a method of UCE [42]. Degrease *Nymphaea hybrid* flowers powder with petroleum ether and weighs 1.0 g. Then *Nymphaea hybrid* flowers powder was mixed with PBS buffer solution (20:1–60:1, mL/g), and adjusted the pH of the solution to

be five. After adding an amount of cellulase (1–5%, *w/w*), the mixture was enzymatically hydrolyzed for 20–100 min at the thermostatic water bath of 50 °C. Then, absolute ethanol was added to the mixture (20–60% ethanol concentration, *v/v*) and the mixture was associated at the ultrasonic power of 150 W and the temperature of 50 °C for 30 min. Finally, the resulting mixture was centrifuged at 10,000 rpm for 15 min. The liquid NHE was separated from the supernatant.

3.4. Flavonoids and Polyphenol Determination

In this study, the total flavonoids were determined using the colorimetric AlCl_3 method [4]. The total flavonoids content was expressed in the dry weight of rutin equivalent and measured absorbance at 415 nm using an ultraviolet spectrophotometer (ALPHA-1860, Puyuan, Shanghai, China). The horizontal coordinate was the concentration of rutin standard, and the vertical coordinate was absorbance to make a five-point calibration line ($y = 0.0078x - 0.0008$, $R^2 = 0.9992$). The total flavonoids of NHE were detected by the above method.

The total polyphenols were determined using the method of Folin–Ciocalteu [64]. It was expressed in the dry weight of gallic acid equivalent and measured absorbance at 760 nm using an ultraviolet spectrophotometer. The horizontal coordinate was the concentration of gallic acid standard, and the vertical coordinate was absorbance to make a five-point calibration line ($y = 0.0431x + 0.0089$, $R^2 = 0.9991$). The total polyphenols of NHE were detected by the above method.

3.5. Response Surface Experiment

Based on single-factor results, Design-Expert software 7.1.3 was used for the experimental design, the result analysis and response prediction. According to the Box–Behnken experiment, the extraction process was optimized by three factors and three levels. The flavonoid content was taken as the index.

3.6. AB-8 Macroporous Resin Experiment

NHE was prepared by the experiment method of the Section 2.3. As an alcohol extract, NHE consisted of a large number of total flavonoids and polyphenols. NHE was purified to obtain NHEP by AB-8 macroporous resin [32,33]. In this experiment, AB-8 macroporous resins are weak polar resins, milk-white spherical particles, and the specific surface area is 480–520 m^2/g . Macroporous resin can be selectively absorbed flavonoids and polyphenols constituents by electrostatic force, hydrogen bonding interactions, complexation and size sieving [45]. Enrichment of these active substances, the flavonoid content of NHE was taken as the index. Different influencing factors were explored to optimize the experiment. Such as AB-8 macroporous resin static/dynamic adsorption and desorption experiments. The influence was tested for adsorption of concentration of NHE (0.33–1.15 mg/mL), pH (2–6) and desorption of ethanol concentration (50–90%) on the static adsorption and desorption experiments, and sample volume (120 mL) and sample flow rate (1.2–7.2 BV/h) on the dynamic experiments. Dynamic experiments: Chromatographic columns: diameter \times length (22 \times 300 mm); the quality of the resin was 5 g; the volume of the resin bed (BV) was 25 mL. Powders of NHE and NHEP, weighing 10.0 mg, was determined the content of polyphenols and flavonoids to test the purification effect of AB-8 macroporous resins. These are examples 2 and 3 of an equation:

$$Q = \frac{C_0 - C_r \times V_0}{m} \quad (2)$$

$$P = \frac{C_d \times V_1}{m} \quad (3)$$

where Q is the absorption capacity of the resin (mg/g), P is the desorption capacity of the resin (mg/g), C_0 and C_r are flavonoids content of NHE at the beginning and at time t

(mg/mL), V_0 is the volume of sample (mL), m is the weight of the resin (g), C_d is flavonoids content of the desorption solution (mg/mL), V_1 is the desorption solution volume (mL).

3.7. Antioxidant and Anti-Inflammatory Activity Analysis

In this study, the raw extract NHE and its purified product NHEP were lyophilized into powder. Their DPPH, ABTS radical scavenging activities and reducing power were measured by an ultraviolet spectrophotometer using VC as the positive control according to the method of Kunnaja et al. [37] and Shaddel et al. [65], respectively. According to the experiment method of Mancarz et al. [66], the anti-inflammatory activity of NHE and NHEP was determined by the inhibition of hyaluronidase activity using dipotassium glycyrrhizinate (Dg) as the positive control.

3.8. Characterization of NHEP by HPLC and FTIR

In this study, the HPLC experiment of the instrument used the Agilent 1260 high-performance liquid chromatography system (Agilent Technologies Inc, Santa Clara, CA, USA). Gallic acid, ellagic acid, rutin, corilagin, myricetin, quercetin, naringin standards and NHEP were determined. The powder of NHEP was prepared to the solution of 1 mg/mL. Chromatographic conditions [29,54,55]: C18 column (4.6 mm \times 250 mm, 5 μ m); mobile phase: 0.1% formic acid in water (A) and acetonitrile (B); gradient elution conditions were 5–13% B for 0–10 min, 13% B for 10–20 min, 13–20% B for 20–35 min, 20–45% B for 35–55 min, 45–100% B for 55–60 min; sample injection volume was 10 μ L; flow rate: 1 mL/min; column temperature: 35 $^{\circ}$ C; detection wavelength: 280 nm.

The powder of NHEP was mixed with spectroscopic KBr, pressed into a sheet for IR analysis using the FTIR spectrometer (Shimadzu Corporation, Shanghai, China) in the range of 4000–500 cm^{-1} [67].

3.9. HaCaT Cell Experiments

The experiment referred to the method of ZHANG J et al. [57,68], the activity of HaCaT cells was determined by the CCK-8 assay. The HaCaT cells of lines growth state were chosen and cultured in DMEM medium containing 10% fetal bovine serum by the culture flask of the adherent cell of 25 cm^2 . The cells were seeded in sterile 96-well plates according to the density of 10,000 per well for 24 h and 48 h into the carbon dioxide incubator at 37 $^{\circ}$ C and 5% CO_2 . The NHEP solution of 1 mg/mL was prepared to remove bacteria and impurities by a 220 nm microporous membrane and the sample was prepared into a mixed medium with a concentration of 10–200 $\mu\text{g}/\text{mL}$. The activity of HaCaT cells was determined by the CCK-8 assay after incubation for 4 h. The optical density (OD) value was measured at the wavelength of 450 nm by the enzyme reader (TECAN, Infinite M200 Pro, Shanghai, China), which was expressed as the percentage of HaCaT cell activity in the control group. Then, the HaCaT cells were seeded in sterile 6-well plates according to the density of 200,000 per well for 24 h and 48 h. The morphology of cells was observed by microscope (Axio Vert.A1, Shanghai, China).

H_2O_2 is one of the ways that induced intracellular production of ROS [69,70]. The HaCaT cells were treated with a nominal concentration of H_2O_2 (25–300 μM) for 2 h. Then, the activity of cells was detected by the CCK-8 assay.

In this experiment, the level of reactive oxygen species (ROS) was detected by a fluorescent probe DCFH-DA in the HaCaT cells [71]. The cells were seeded in black sterile 96-well plates according to the density of 10,000 per well. After 24 h of culture in the mixed medium of the NHEP of 10–160 $\mu\text{g}/\text{mL}$, HaCaT cells were stimulated with 100 μM H_2O_2 for 2 h. Then, the cells were mixed with the DCFH-DA fluorescent probe for 30 min. The fluorescence intensity was detected at the excitation wavelength of 488 nm and the emission wavelength of 525 nm, which was expressed as the percentage of ROS in the control group of HaCaT cells.

3.10. B16 Mouse Melanoma Cells Experiments

The experiment referred to the method of AIMVIJARN P et al. [63], the activity of B16 cells was determined by the CCK-8 assay. The cells were seeded in sterile 96-well plates according to the density of 6000 per well for 24 h and 48 h. The samples were prepared into a mixed medium with a concentration of 10–140 µg/mL. Then, the B16 cells were seeded in sterile 6-well plates according to the density of 100,000 per well for 24 h and 48 h. The morphology of cells was observed by microscope.

The melanin content of B16 cells was detected by referring to the method of Teng et al. [62] The sample was mixed medium with a concentration of 10–80 µg/mL. The B16 cells were seeded in sterile 6-well plates according to the density of 100,000 per well for 72 h. Then, the cells were separated by trypsinization and disrupted by using 10% DMSO with 1 M NaOH at 80 °C for 1 h. The melanin content was determined at 405 nm, which was expressed as the percentage of melanin content in the control group of B16 cells.

3.11. Statistical Analysis

Design-Expert software 7.1.3 was used for response surface analyses. Other Statistical analyses were performed with OriginPro 2021b. All experiments tested replicate at least three times. The significant represented that sample group compared with the control group, $p < 0.05$, $p < 0.01$ and $p < 0.001$ were performed *, ** and ***, respectively. The data shows the mean \pm S.D.

4. Conclusions

In this paper, ultrasound-assisted cellulase extraction method associated with macroporous resin purification step was successfully applied to enrich antioxidant flavonoids and polyphenols from *Nymphaea hybrid* flowers for the first time. The optimum extraction conditions obtained by RSM were as follows: liquid-to-solid ratio of 40.45:1 (mL/g), cellulase ratio of 4.23%, and ethanol concentration of 52%. After purification by macroporous resins, the flavonoid content increased from 55.60 mg/g (NHE) to 157.37 mg/g (NHEP), and the polyphenols content increased from 414.97 mg/g (NHE) to 888.63 mg/g (NHEP), respectively. Seven major flavonoids or polyphenols in NHEP were identified and quantified by the HPLC method. The chemical evaluation method of the antioxidant and anti-inflammatory effect of NHEP was determined by scavenging free radicals (DPPH, ABTS), reduction power and inhibiting hyaluronidase assay. The intracellular antioxidant and whitening effects of NHEP on HaCaT cells and B16 cells were detected. These experiments results indicated that the NHEP displayed significantly antioxidant, whitening, anti-inflammatory effects and the protective effect against H₂O₂-induced oxidative damage in human cells, which promote the potential as a functional raw material in the field of cosmetics and medicine.

Author Contributions: Conceptualization, H.-M.L. and S.-N.L.; methodology, H.-M.L. and S.-N.L.; software, S.-N.L. and W.T.; validation, S.-N.L., W.T. and Z.-W.Z.; formal analysis, S.-N.L., M.-H.X. and M.-Y.C.; investigation, H.-M.L. and X.-D.Z.; resources, H.-M.L. and W.W.; data curation, S.-N.L.; writing—original draft preparation, S.-N.L.; writing—review and editing, S.-N.L. and H.-M.L.; visualization, S.-N.L.; supervision, W.W.; project administration, H.-M.L. and W.W.; funding acquisition, H.-M.L. and W.W. All authors have read and agreed to the published version of the manuscript.

Funding: This research was funded by Shanghai Alliance Program (LM201941).

Institutional Review Board Statement: Not applicable.

Informed Consent Statement: Not applicable.

Data Availability Statement: Data are contained within the article.

Conflicts of Interest: The authors declare no conflict of interest.

Sample Availability: Samples of the extraction of *Nymphaea hybrid* are available from the authors.

References

1. Zhang, H.; Wu, H.; Zhou, Q.; Zhao, R.; Sheng, Q.; Zhu, Z. Flowering characteristics and reproductive biology of *Nymphaea* hybrid, a precious water lily. *Sci. Hortic.* **2021**, *287*, 110268. [[CrossRef](#)]
2. Nierbauer, K.U.; Kanz, B.; Zizka, G. The widespread naturalisation of *Nymphaea* hybrids is masking the decline of wild-type *Nymphaea alba* in Hesse, Germany. *Flora Morphol. Distrib. Funct. Ecol. Plants* **2014**, *209*, 122–130. [[CrossRef](#)]
3. Rasid, N.S.A.; Naim, M.N.; Man, H.C.; Bakar, N.F.A.; Mokhtar, M.N. Evaluation of surface water treated with lotus plant; *Nelumbo nucifera*. *J. Environ. Chem. Eng.* **2019**, *7*, 103048. [[CrossRef](#)]
4. Tungmunnithum, D.; Drouet, S.; Kabra, A.; Hano, C. Enrichment in Antioxidant Flavonoids of Stamen Extracts from *Nymphaea lotus* L. Using Ultrasonic-Assisted Extraction and Macroporous Resin Adsorption. *Antioxidants* **2020**, *9*, 576. [[CrossRef](#)] [[PubMed](#)]
5. Alam, M.B.; Ahmed, A.; Motin, M.A.; Kim, S.; Lee, S.H. Attenuation of melanogenesis by *Nymphaea nouchali* (Burm. f) flower extract through the regulation of cAMP/CREB/MAPKs/MITF and proteasomal degradation of tyrosinase. *Sci. Rep.* **2018**, *8*, 13928. [[CrossRef](#)] [[PubMed](#)]
6. Cudalbeanu, M.; Peitinho, D.; Silva, F.; Marques, R.; Pinheiro, T.; Ferreira, A.C.; Marques, F.; Paulo, A.; Soeiro, C.F.; Sousa, S.A.; et al. Sono-Biosynthesis and Characterization of AuNPs from Danube Delta *Nymphaea alba* Root Extracts and Their Biological Properties. *Nanomaterials* **2021**, *11*, 1562. [[CrossRef](#)] [[PubMed](#)]
7. Jahan, I.; Mamun, M.; Hossen, M.A.; Sakir, J.; Haque, M.E. Antioxidant, Analgesic and Anti-Inflammatory Activities of *Nymphaea Nouchali* Flowers. *Res. J. Pharmacol.* **2012**, *6*, 62–70.
8. Oyeyemi, I.T.; Akanni, O.O.; Adaramoye, O.A.; Bakare, A.A. Methanol extract of *Nymphaea lotus* ameliorates carbon tetrachloride-induced chronic liver injury in rats via inhibition of oxidative stress. *J. Basic Clin. Physiol. Pharm.* **2017**, *28*, 43–50. [[CrossRef](#)] [[PubMed](#)]
9. Chaurasia, S.; Sharma, V.; Dar, A.I.; Neetu Arya, R.C.S.; Chaurasia, I.D.; Shrivastava, R. In-vivo Antidiabetic activity of Alcoholic and Aqueous Extract of *Nymphaea lotus* in Rat Model. *Inven. Rapid: Ethnopharmacol.* **2011**, *3*, 2.
10. Acharya, J.; Dutta, M.; Chaudhury, K.; De, B. Metabolomics and chemometric study for identification of acetylcholinesterase inhibitor(s) from the flower extracts of *Nymphaea pubescens*. *J. Food Biochem.* **2018**, *42*, e12575. [[CrossRef](#)]
11. Ordonez, A.; Gomez, J.; Vattuone, M.; Lsla, M. Antioxidant activities of *Sechium edule* (Jacq.) Swartz extracts. *Food Chem.* **2006**, *97*, 452–458. [[CrossRef](#)]
12. Mita, R.N.L.P.; Amir, H. Antioxidant activity of methanolic extract of *Eucheuma spinosum* extracted using a microwave. *IOP Conf. Ser. Earth Environ. Sci.* **2021**, *763*, 012028.
13. El-Roby, A.M.; Hammad, K.S.M.; Galal, S.M. Enhancing oxidative stability of sunflower oil with sesame (*Sesamum indicum*) coat ultrasonic extract rich in polyphenols. *J. Food Processing Preserv.* **2020**, *44*, 8. [[CrossRef](#)]
14. Salehi, H.; Karimi, M.; Raofie, F. Micronization and coating of bioflavonoids extracted from *Citrus sinensis* L. peels to preparation of sustained release pellets using supercritical technique. *J. Iran. Chem. Soc.* **2021**, *18*, 1–14. [[CrossRef](#)]
15. Ines, I.M.; Arturo, R.J.; Sandra, D.M.; Montserrat, C.; Guadalupe, A.M. Enzymatic hydrolysis of lignocellulosic biomass using native cellulase produced by *Aspergillus niger* ITV02 under liquid state fermentation. *Biotechnol. Appl. Biochem.* **2021**, *69*, 198–208.
16. Drevelegka, I.; Goula, A.M. Recovery of grape pomace phenolic compounds through optimized extraction and adsorption processes. *Chem. Eng. Processing Process Intensif.* **2020**, *149*, 107845. [[CrossRef](#)]
17. Hu, B.; Li, Y.; Song, J.; Li, H.; Zhou, Q.; Li, C.; Zhang, Z.; Liu, Y.; Liu, A.; Zhang, Q.; et al. Oil extraction from tiger nut (*Cyperus esculentus* L.) using the combination of microwave-ultrasonic assisted aqueous enzymatic method-design, optimization and quality evaluation. *J. Chromatogr. A* **2020**, *1627*, 461380. [[CrossRef](#)]
18. Tran, D.D.; Hoang, L.D.; Tai, N.; Thi, P.M.T.; My, P.L.T.; Thanh, V.H.; Viet, N.D.; Thuy, L.N.T.; Nam, H.M.; Phong, M.T.; et al. Utilization of Response Surface Methodology in Optimization of Polysaccharides Extraction from Vietnamese Red by Ultrasound-Assisted Enzymatic Method and Examination of Bioactivities of the Extract. *Sci. World J.* **2021**, *11*, 7594092.
19. Costa-Junior, R.B.; Brandao-Costa, R.M.P.; Albuquerque, W.W.C.; Batista, J.M.S.; Pedrosa, R.B.; Porto, A.L.F. Ultrasound-Assisted Enzyme-Catalyzed Hydrolysis of Collagen to Produce Peptides with Biomedical Potential: Collagenase From *Aspergillus terreus* UCP1276. *Bioelectromagnetics* **2020**, *41*, 113–120. [[CrossRef](#)]
20. Xu, X.Y.; Meng, J.M.; Mao, Q.Q.; Shang, A.; Li, B.Y.; Zhao, C.N.; Tang, G.Y.; Cao, S.Y.; Wei, X.L.; Gan, R.Y.; et al. Effects of Tannase and Ultrasound Treatment on the Bioactive Compounds and Antioxidant Activity of Green Tea Extract. *Antioxidants* **2019**, *8*, 362. [[CrossRef](#)]
21. Zhao, F.; Li, X. Ultrasonic-assisted enzymatic extraction of silymarin from the *Silybum marianum* seed shell and evaluation of its antioxidant activity in vitro. *EXCLI J.* **2015**, *14*, 861–874. [[CrossRef](#)] [[PubMed](#)]
22. Hu, B.; Wang, H.; He, L.; Li, Y.; Li, C.; Zhang, Z.; Liu, Y.; Zhou, K.; Zhang, Q.; Liu, A.; et al. A method for extracting oil from cherry seed by ultrasonic-microwave assisted aqueous enzymatic process and evaluation of its quality. *J. Chromatogr. A* **2019**, *1587*, 50–60. [[CrossRef](#)] [[PubMed](#)]
23. Xue, H.; Tan, J.; Li, Q.; Tang, J.; Cai, X. Ultrasound-Assisted Enzymatic Extraction of Anthocyanins from Raspberry Wine Residues: Process Optimization, Isolation, Purification, and Bioactivity Determination. *Food Anal. Methods* **2021**, *14*, 1369–1386. [[CrossRef](#)]
24. Xu, Y.; Zhang, L.; Yang, Y.; Song, X.; Yu, Z. Optimization of ultrasound-assisted compound enzymatic extraction and characterization of polysaccharides from blackcurrant. *Carbohydr. Polym.* **2015**, *117*, 895–902. [[CrossRef](#)] [[PubMed](#)]

25. Ke, L.-Q. Optimization of Ultrasonic Extraction of Polysaccharides from *Lentinus Edodes* Based on Enzymatic Treatment. *J. Food Processing Preserv.* **2015**, *39*, 254–259. [[CrossRef](#)]
26. Liu, Y.; Gong, G.; Zhang, J.; Jia, S.; Li, F.; Wang, Y.; Wu, S. Response surface optimization of ultrasound-assisted enzymatic extraction polysaccharides from *Lycium barbarum*. *Carbohydr. Polym.* **2014**, *110*, 278–284. [[CrossRef](#)] [[PubMed](#)]
27. Bi, W.; Yoon, C.H.; Row, K.H. Ultrasonic-Assisted Enzymatic Ionic Liquid-Based Extraction and Separation of Flavonoids from *Chamaecyparis Obtusa*. *J. Liq. Chromatogr. Relat. Technol.* **2013**, *36*, 2029–2043. [[CrossRef](#)]
28. Sharma, A.; Gupta, M.N. Ultrasonic pre-irradiation effect upon aqueous enzymatic oil extraction from almond and apricot seeds. *Ultrason. Sonochem.* **2006**, *13*, 529–534. [[CrossRef](#)] [[PubMed](#)]
29. Cudalbeanu, M.; Ghinea, I.O.; Furdul, B.; Dah-Nouvlessounon, D.; Raclea, R.; Costache, T.; Cuculea, I.E.; Urgan, F.; Dinica, R.M. Exploring New Antioxidant and Mineral Compounds from *Nymphaea alba* Wild-Grown in Danube Delta Biosphere. *Molecules* **2018**, *23*, 1247. [[CrossRef](#)] [[PubMed](#)]
30. Zhu, M.Z.; Wu, W.; Jiao, L.L.; Yang, P.F.; Guo, M.Q. Analysis of Flavonoids in Lotus (*Nelumbo nucifera*) Leaves and Their Antioxidant Activity Using Macroporous Resin Chromatography Coupled with LC-MS/MS and Antioxidant Biochemical Assays. *Molecules* **2015**, *20*, 10553–10565. [[CrossRef](#)]
31. Mariotti-Celis, M.S.; Martínez-Cifuentes, M.; Huamán-Castilla, N.; Pedreschi, F.; Iglesias-Rebolledo, N.; Pérez-Correa, J.R. Impact of an integrated process of hot pressurised liquid extraction-macroporous resin purification over the polyphenols, hydroxymethylfurfural and reducing sugars content of *Vitis vinifera* ‘Carménère’ pomace extracts. *Int. J. Food Sci. Technol.* **2018**, *53*, 1072–1078. [[CrossRef](#)]
32. Limwachiranon, J.; Huang, H.; Li, L.; Duan, Z.; Luo, Z. Recovery of lotus (*Nelumbo nucifera* Gaertn.) seedpod flavonoids using polar macroporous resins: The updated understanding on adsorption/desorption mechanisms and the involved intermolecular attractions and bonding. *Food Chem.* **2019**, *299*, 125108. [[CrossRef](#)] [[PubMed](#)]
33. Xiaoyong, W.; Yuan, T.; Yanxia, S.; Dabing, X.; Yan, W.; Qi, W.; Gang, Z. Retracted Article: Extraction of flavonoids and kinetics of purification by macroporous resins from quinoa. *J. Nanoparticle Res.* **2020**, *22*, 181. [[CrossRef](#)]
34. Yang, X.; Bai, Z.F.; Zhang, D.W.; Zhang, Y.; Cui, H.; Zhou, H.L. Enrichment of flavonoid-rich extract from *Bidens bipinnata* L. by macroporous resin using response surface methodology, UHPLC-Q-TOF MS/MS-assisted characterization and comprehensive evaluation of its bioactivities by analytical hierarchy process. *Biomed. Chromatogr.* **2020**, *34*, e4933. [[CrossRef](#)] [[PubMed](#)]
35. Wu, Y.; Jiang, Y.; Zhang, L.; Zhou, J.; Yu, Y.; Zhang, S.; Zhou, Y. Green and efficient extraction of total glucosides from *Paeonia lactiflora* Pall. ‘Zhongjiang’ by subcritical water extraction combined with macroporous resin enrichment. *Ind. Crops Prod.* **2019**, *141*, 111699. [[CrossRef](#)]
36. Sklirou, A.D.; Angelopoulou, M.T.; Argyropoulou, A.; Chaita, E.; Boka, V.I.; Cheimonidi, C.; Niforou, K.; Mavrogonatou, E.; Pratsinis, H.; Kalpoutzakis, E.; et al. Phytochemical Study and In Vitro Screening Focusing on the Anti-Aging Features of Various Plants of the Greek Flora. *Antioxidants* **2021**, *10*, 1206. [[CrossRef](#)]
37. Kunnaja, P.; Chansakaow, S.; Wittayapraparat, A.; Yusuk, P.; Sireeratawong, S. In Vitro Antioxidant Activity of *Litsea martabanica* Root Extract and Its Hepatoprotective Effect on Chlorpyrifos-Induced Toxicity in Rats. *Molecules* **2021**, *26*, 1906. [[CrossRef](#)]
38. Cosin-Tomas, M.; Senserrich, J.; Arumi-Planas, M.; Alquezar, C.; Pallas, M.; Martín-Requero, A.; Sunol, C.; Kaliman, P.; Sanfeliu, C. Role of Resveratrol and Selenium on Oxidative Stress and Expression of Antioxidant and Anti-Aging Genes in Immortalized Lymphocytes from Alzheimer’s Disease Patients. *Nutrients* **2019**, *11*, 1764. [[CrossRef](#)]
39. Schaich, K.M.; Tian, X.; Xie, J. Hurdles and pitfalls in measuring antioxidant efficacy: A critical evaluation of ABTS, DPPH, and ORAC assays. *J. Funct. Foods* **2015**, *14*, 111–125. [[CrossRef](#)]
40. Nwachukwu, I.D.; Sarteshnizi, R.A.; Udenigwe, C.C.; Aluko, R.E. A Concise Review of Current In Vitro Chemical and Cell-Based Antioxidant Assay Methods. *Molecules* **2021**, *26*, 4865. [[CrossRef](#)]
41. Li, Y.L.; Chen, X.; Niu, S.Q.; Zhou, H.Y.; Li, Q.S. Protective Antioxidant Effects of Amentoflavone and Total Flavonoids from *Hedyotis diffusa* on H₂O₂-Induced HL-O2 Cells through ASK1/p38 MAPK Pathway. *Chem. Biodivers.* **2020**, *17*, e2000251. [[CrossRef](#)] [[PubMed](#)]
42. Wu, D.; Gao, T.; Yang, H.; Du, Y.; Li, C.; Wei, L.; Zhou, T.; Lu, J.; Bi, H. Simultaneous microwave/ultrasonic-assisted enzymatic extraction of antioxidant ingredients from *Nitraria tangutorun* Bobr. juice by-products. *Ind. Crops Prod.* **2015**, *66*, 229–238. [[CrossRef](#)]
43. Huang, D.; Zhou, X.; Si, J.; Gong, X.; Wang, S. Studies on cellulase-ultrasonic assisted extraction technology for flavonoids from *Illicium verum* residues. *Chem. Cent. J.* **2016**, *10*, 56. [[CrossRef](#)] [[PubMed](#)]
44. Laffort, P. A Revisited Definition of the Three Solute Descriptors Related to the Van der Waals Forces in Solutions. *Open J. Phys. Chem.* **2016**, *6*, 86–100. [[CrossRef](#)]
45. Xi, L.; Mu, T.; Sun, H. Preparative purification of polyphenols from sweet potato (*Ipomoea batatas* L.) leaves by AB-8 macroporous resins. *Food Chem.* **2015**, *172*, 166–174. [[CrossRef](#)] [[PubMed](#)]
46. Zhou, P.; Fangma, Y.; Jin, W.; Jin, Z.; Li, X.; He, Y. Response surface optimization of the water immersion extraction and macroporous resin purification processes of anhydrosafflor yellow B from *Carthamus tinctorius* L. *J. Food Sci.* **2020**, *85*, 3191–3201. [[CrossRef](#)] [[PubMed](#)]

47. Jia, G.; Lu, X. Enrichment and purification of madecassoside and asiaticoside from *Centella asiatica* extracts with macroporous resins. *J. Chromatogr. A* **2008**, *1193*, 136–141. [[CrossRef](#)] [[PubMed](#)]
48. Gomathi, D.; Ravikumar, G.; Kalaiselvi, M.; Vidya, B.; Uma, C. In Vitro Free Radical Scavenging Activity of Ethanolic Extract of the Whole Plant of *Evolvulus alsinoides* (L.) L. *Chin. J. Integr. Med.* **2015**, *21*, 453–458. [[CrossRef](#)] [[PubMed](#)]
49. Santos, J.; Pereira, J.; Ferreira, N.; Paiva, N.; Ferra, J.; Magalhães, F.D.; Martins, J.M.; Dulyanska, Y.; Carvalho, L.H. Valorisation of non-timber by-products from maritime pine (*Pinus pinaster*, Ait) for particleboard production. *Ind. Crops Prod.* **2021**, *168*. [[CrossRef](#)]
50. García, D.E.; Delgado, N.; Aranda, F.L.; Toledo, M.A.; Cabrera-Barjas, G.; Sintjago, E.M.; Escobar-Avello, D.; Paczkowski, S. Synthesis of maleilated polyflavonoids and lignin as functional bio-based building-blocks. *Ind. Crops Prod.* **2018**, *123*, 154–163. [[CrossRef](#)]
51. Escobar-Avello, D.; Avendano-Godoy, J.; Santos, J.; Lozano-Castellon, J.; Mardones, C.; von Baer, D.; Luengo, J.; Lamuela-Raventos, R.M.; Vallverdu-Queralt, A.; Gomez-Gaete, C. Encapsulation of Phenolic Compounds from a Grape Cane Pilot-Plant Extract in Hydroxypropyl Beta-Cyclodextrin and Maltodextrin by Spray Drying. *Antioxidants* **2021**, *10*, 1130. [[CrossRef](#)] [[PubMed](#)]
52. Dubey, P.; Sharma, P.; Kumar, V. Structural profiling of wax biopolymer from *Pinus roxburghii* Sarg. needles using spectroscopic methods. *Int. J. Biol. Macromol.* **2017**, *104*, 261–273. [[CrossRef](#)] [[PubMed](#)]
53. Felhi, S.; Hajlaoui, H.; Ncir, M.; Bakari, S.; Ktari, N.; Saoudi, M.; Gharsallah, N.; Kadri, A. Nutritional, phytochemical and antioxidant evaluation and FT-IR analysis of freeze dried extracts of *Ecballium elaterium* fruit juice from three localities. *Food Sci. Technol.* **2016**, *36*, 646–655. [[CrossRef](#)]
54. Uddin, M.N.; Samad, M.A.; Zubair, M.A.; Haque, M.Z.; Mitra, K.; Khan, T.; Hossain, M.; Syed, A.; Afroze, A. Potential bioactive phytochemicals, antioxidant properties and anticancer pathways of *Nymphaea nouchali*. *Asian Pac. J. Trop. Bio.* **2020**, *10*, 555–562. [[CrossRef](#)]
55. Gunhyuk, P.; Yeomoon, S.; Wonil, L.; Hyun, S.S.; Sook, O.M. Protection on Skin Aging Mediated by Antiapoptosis Effects of the Water Lily (*Nymphaea Tetragona* Georgi) via Reactive Oxygen Species Scavenging in Human Epidermal Keratinocytes. *Pharmacology* **2016**, *97*, 282–293.
56. Medrano-Padial, C.; Puerto, M.; Moreno, F.J.; Richard, T.; Cantos-Villar, E.; Pichardo, S. In Vitro Toxicity Assessment of Stilbene Extract for Its Potential Use as Antioxidant in the Wine Industry. *Antioxidants* **2019**, *8*, 467. [[CrossRef](#)] [[PubMed](#)]
57. Zhang, J.; Wang, W.; Mao, X. Chitopentaose protects HaCaT cells against H₂O₂-induced oxidative damage through modulating MAPKs and Nrf2/ARE signaling pathways. *J. Funct. Foods* **2020**, *72*, 104086. [[CrossRef](#)]
58. Chang, T.M.; Tsen, J.H.; Yen, H.; Yang, T.Y.; Huang, H.C. Extract from *Periostracum cicadae* Inhibits Oxidative Stress and Inflammation Induced by Ultraviolet B Irradiation on HaCaT Keratinocytes. *Evid. Based Complementary Altern. Med.* **2017**, *2017*, 8325049. [[CrossRef](#)] [[PubMed](#)]
59. Dias, V.; Junn, E.; Mouradian, M.M. The role of oxidative stress in Parkinson's disease. *J. Parkinsons Dis.* **2013**, *3*, 461–491. [[CrossRef](#)]
60. Hou, D.-X. Potential Mechanisms of Cancer Chemoprevention by Anthocyanins. *Curr. Mol. Med.* **2003**, *3*, 149–159. [[CrossRef](#)] [[PubMed](#)]
61. Diaconeasa, Z.; Leopold, L.; Rugina, D.; Ayvaz, H.; Socaciu, C. Antiproliferative and antioxidant properties of anthocyanin rich extracts from blueberry and blackcurrant juice. *Int. J. Mol. Sci.* **2015**, *16*, 2352–2365. [[CrossRef](#)] [[PubMed](#)]
62. Teng, H.; Fan, X.; Lv, Q.; Zhang, Q.; Xiao, J.; Qian, Y.; Zheng, B.; Gao, H.; Gao, S.; Chen, L. *Folium nelumbinis* (Lotus leaf) volatile-rich fraction and its mechanisms of action against melanogenesis in B16 cells. *Food Chem.* **2020**, *330*, 127030. [[CrossRef](#)] [[PubMed](#)]
63. Aimvijarn, P.; Rodboon, T.; Payuhakrit, W.; Suwannalert, P. *Nymphaea pubescens* Induces Apoptosis, Suppresses Cellular Oxidants-Related Cell Invasion in B16 Melanoma Cells. *Pharm. Sci.* **2018**, *24*, 199–206. [[CrossRef](#)]
64. Parimala, M.; Shoba, F.G. Phytochemical analysis and In vitro antioxidant activity of hydroalcoholic seed extract of *Nymphaea nouchali* Burm. f. *Asian Pac. J. Trop. Biomed.* **2013**, *3*, 887–895. [[CrossRef](#)]
65. Shaddel, R.; Maskooki, A.; Haddad-Khodaparast, M.H.; Azadmard-Damirchi, S.; Mohamadi, M.; Fathi-Achachlouei, B. Optimization of extraction process of bioactive compounds from Bene hull using subcritical water. *Food Sci. Biotechnol.* **2014**, *23*, 1459–1468. [[CrossRef](#)]
66. Mancarz, G.F.F.; Laba, L.C.; Morais Silva, T.A.; Pazzim, M.D.S.; de Souza, D.; Prado, M.R.M.; de Souza, L.M.; Nakashima, T.; Mello, R.G. Chemical composition and biological activity of Liquidambar styraciflua L. leaf essential oil. *Ind. Crops Prod.* **2019**, *138*, 111446. [[CrossRef](#)]
67. Jesse, A.O. Fourier Transform Infrared Spectroscopy Analysis of *Allium sativum* L. and *Nymphaea lotus* L. *Asian J. Appl. Chem. Res.* **2020**, *6*, 7–24. [[CrossRef](#)]
68. Liu, H.M.; Xu, P.F.; Cheng, M.Y.; Lei, S.N.; Liu, Q.L.; Wang, W. Optimization of Fermentation Process of Pomegranate Peel and Schisandra Chinensis and the Biological Activities of Fermentation Broth: Antioxidant Activity and Protective Effect Against H₂O₂-induced Oxidative Damage in HaCaT Cells. *Molecules* **2021**, *26*, 3432. [[CrossRef](#)]
69. Song, I.B.; Gu, H.; Han, H.J.; Lee, N.Y.; Cha, J.Y.; Son, Y.K.; Kwon, J. Effects of 7-MEGA(TM) 500 on Oxidative Stress, Inflammation, and Skin Regeneration in H₂O₂-Treated Skin Cells. *Toxicol. Res.* **2018**, *34*, 103–110. [[CrossRef](#)]

70. Zanoni, T.B.; Hudari, F.; Munnia, A.; Peluso, M.; Godschalk, R.W.; Zanoni, M.V.; den Hartog, G.J.; Bast, A.; Barros, S.B.; Maria-Engler, S.S.; et al. The oxidation of p-phenylenediamine, an ingredient used for permanent hair dyeing purposes, leads to the formation of hydroxyl radicals: Oxidative stress and DNA damage in human immortalized keratinocytes. *Toxicol. Lett.* **2015**, *239*, 194–204. [[CrossRef](#)]
71. Lee, H.; Yeom, M.; Shin, S.; Jeon, K.; Park, D.; Jung, E. Protective Effects of Aqueous Extract of *Mentha suaveolens* against Oxidative Stress-Induced Damages in Human Keratinocyte HaCaT Cells. *Evid. Based Complementary Altern. Med.* **2019**, *2019*, 5045491. [[CrossRef](#)] [[PubMed](#)]